LANDSLIDES IN NORTHEASTERN MINNESOTA:
Inventory Mapping and Susceptibility Assessment

A THESIS
SUBMITTED TO THE FACULTY OF THE
UNIVERSITY OF MINNESOTA
BY

Emilie M. Richard

IN PARTIAL FULFILLMENT OF THE REQUIREMENTS
FOR THE DEGREE OF
MASTER OF SCIENCE

Dr. Karen Gran

December 2020

Acknowledgements

There are many people to thank for their contributions throughout this project. I'd like to express sincere gratitude to my advisor and mentor, Dr. Karen Gran, whose guidance is empowering and continues to inspire me. To my committee members, Dr. Stephen DeLong, Dr. John Swenson, and Dr. Tongxin Zhu, thank you for asking all the right questions and helping me answer them. Thank you to Carrie Jennings, Andy Breckenridge, and the rest of the Minnesota Landslides Project team for your collaboration and insight. Thank you to my undergraduate research assistants, Derek Dahly and Rayann Rehwinkel, who endured long days hiking through the woods with me and ran in the right direction when I screamed "bees!". To Zachary Engle and Brian Scott, thank you for helping me tackle countless GIS and coding conundrums. Special thanks to Brian Sockness, Larissa Scott and Emma Burgeson for being amazing sounding boards for my thoughts throughout this process and helping me get through 2020 with most of my sanity. Finally, to my friends and family, thank you all for diffusing my mis-directed stress and always keeping me grounded. You are my favorite rock collection.

Funding for this project was provided by the Minnesota Environment and Natural Resources Trust Fund as recommended by the Legislative-Citizen Commission on Minnesota Resources (LCCMR).

Abstract

Landslides and other mass-movement events are common geomorphic phenomena in Minnesota that threaten water quality, infrastructure, and public safety. Most published studies on the subject are geographically biased to mountainous regions, and little research has focused on low-relief landscapes like the central lowlands of the United States. This study focuses on slope instability across northeastern Minnesota as part of a collaborative, nearly statewide, landslide inventory and susceptibility mapping project. I developed a database of 2,005 remotely-mapped slope failures from historical records, lidar data, and aerial imagery using GIS software. Field verification of 702 slides determined that remote mapping was approximately 97% accurate. To develop a landslide susceptibility map, I applied a logistic regression (LR) analysis using a set of nine predictive independent variables that may impact slope stability (slope, aspect, elevation, relief, depth to bedrock, soil erodibility, substrate, land cover, and distance to streams). The multivariate LR analyses utilized landslide inventories from two separate study areas that represented different scales and paleogeomorphic settings for comparison: Jay Cooke State Park (JCSP)(32.8 km^2) and the Lake Superior South watershed (LSSW)(1,628 km^2). The JCSP area along the St. Louis River contains glaciolacustrine sediments and shoreline deposits from pro-glacial lake Duluth, and the LSSW hosts subglacial and ice-marginal moraine deposits from the Superior Lobe. Data sampled from the landslide inventories were subdivided into 80% training and 20% test data in each area. Confusion matrices, comparing model predictions to actual inventory data, were used to assess model accuracy. I found that slope, depth to bedrock, distance to streams, and substrate were statistically significant variables to predict landslides in a multivariate LR analysis in both test areas, though slope alone was a strong enough variable to predict the majority of landslides. Models were more accurate at a scale similar to the resolution of the state datasets used in the analysis (83% in JCSP; 95% in LSSW). The models' transferability was then tested in a third study area, the Mission Creek watershed (28.5 km^2) an area adjacent to JCSP with similar surficial material and different bedrock. The JCSP model performed with higher accuracy (92%) than the LSSW model (56%) at predicting landslides in the Mission Creek Watershed. Model

comparisons revealed the importance of considering paleogeomorphic settings such as ice-margins, glacial lake-basins, or shoreline environments on landslide susceptibility and occurrence. Outcomes from this research lay the groundwork for future studies across the state and allow stakeholders to reduce risks from future landslides in the face of a changing climate.

Table of Contents

List of Tables

List of Figures

Introduction

Slope failure is a major geomorphic process that occurs on all continents, naturally reshaping landscapes through episodic erosion. The more commonly used term "landslide" is synonymous with "slope failure" or "mass-wasting", all of which describe the mass movement of rock, debris, or earth downslope (Highland and Browbowsky, 2008). Mass-wasting events become geologic hazards when they are associated with public safety, infrastructure, and environmental degradation. Across the United States, landslides are responsible for 25–50 deaths annually and damages exceeding $2 billion per year (Schuster and Fleming, 1986; Spiker and Gori, 2000). To resolve the resource management challenges associated with landslides and related phenomena, we must enhance our understanding of where they occur and the geoenvironmental factors that drive them.

Comprehensive landslide detection and mapping are the basis for any landslide susceptibility assessment (Carrara and Merenda, 1976; Guzzetti et al., 2000; Brardinoni et al., 2003; Martha et al., 2010). Landslide susceptibility is the probability of slope failure based on local geoenvironmental conditions, assuming that future slopes will fail under the same conditions that destabilized them in the past (Guzzetti et al., 2006). Landslide inventory and susceptibility mapping has grown and evolved over the past two decades as high-resolution airborne lidar data become more widespread and geoprocessing technologies advance. Despite the abundance of research on landslide susceptibility mapping, studies are geographically biased with a greater emphasis on tectonically-active mountainous regions (Reichenbach et al., 2018). Little research has been published on landslide susceptibility in lower-gradient landscapes like the central lowlands of the United States.

In Minnesota, where the majority of mass-wasting events occur along river valleys, bluff erosion is a primary contributor to sediment loading in streams and rivers (Sekely et al., 2002; Belmont, 2011; Day et al., 2013; Lahti et al., 2013; Wick, 2013; Neitzel, 2014; Hall, 2016; Sandberg et al., 2017; Jasperson et al., 2018). Excess sediment in streams has the potential to raise water temperatures, decrease the biodiversity of macroinvertebrates, and negatively affect fish life-cycles (Castro and Reckendorf, 1995).

Despite the propensity for bluff erosion along Minnesota streams and the implications for water quality, the state lacks a comprehensive landslide hazards map and mitigation protocol. Recently deglaciated landscapes contain evidence of their historic depositional environments that translate to differences in substrate, surficial sediment thickness, proximity to streams/lakeshore, and topography which could be uniquely important factors influencing slope failures. These geomorphic boundaries, such as sub-glacial environments, ice-marginal settings, outwash plains, paleo-shoreline deposits, and glacial lake beds, could affect the scale and transferability of susceptibility models.

This research is part of a larger project funded by the Legislative-Citizen Commission of Minnesota Resources (LCCMR) to assess landslide hazards and impacts across the state of Minnesota (Gran, 2017). My research focused specifically on documenting slope failures throughout the Lake Superior watershed to generate an inventory of landslides that served as the basis for landslide susceptibility assessments using a logistic regression (LR) statistical analysis. I investigated this by selecting two study areas of different sizes within different glacial depositional environments: Jay Cooke State Park (32.8 km^2) and the Lake Superior South watershed (1628 km^2). A third study area (the Mission Creek watershed (28.5 km^2)) was used to compare how these two predictive models performed in a different setting where no susceptibility analysis was conducted.

Landslides are essential mechanisms of landscape evolution, though they are often perceived as rare catastrophic events. While these catastrophic failures are visibly destructive and receive more media coverage, the compounding effects from hundreds of smaller failures should not be overlooked. The findings from this project will help stakeholders make informed management decisions to protect individuals and property from mass movements while preserving local ecosystems, fisheries, and recreation associated with Minnesota's treasured waters.

Background

Slope Stability Mechanics

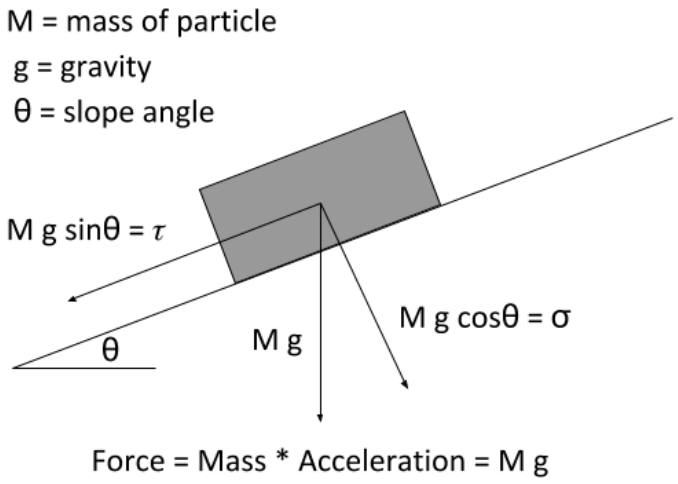

Figure 1. Slope stability schematic diagram for a particle on a shallow planar surface.

The potential of material on a slope to withstand movement is quantified in terms of slope stability, or the balance between driving forces that promote movement and resisting forces that deter movement. In northeastern Minnesota, we are concerned with the slope stability of unconsolidated material on shallow planar surfaces. The primary driving force is the downslope component of gravity, known as the shear stress (τ) [Figure 1]. The main resisting force is the shear strength, which depends on the normal stress (σ), angle of internal friction ($\emptyset$), and cohesion of the material (c) (Ritter et al., 2002). Normal stress considers both the effective normal stress (σ') and pore pressure (μ). The effective normal stress is the stress exerted at the solid-to-solid contacts along a shear surface and pore pressure is the pressure within void spaces of the material. The angle of internal friction is the angle at which material will begin to slide and is an intrinsic property of the material. Cohesion (the strength of the force that holds particles together) changes based on material composition and the presence or absence of moisture.

A slope is considered stable when the sum of the applied shear stresses does not exceed the material's shear strength. This ratio of shear strength over shear stress is referred to as the factor of safety (F_s) and one example of this is the infinite slope model.

$$F_s = \frac{\sum Resisting\ Forces\ (shear\ strength)}{\sum Driving\ Forces\ (shear\ stress)} = \frac{c + \sigma' tan\emptyset}{\tau} \qquad (1)$$

As the factor of safety gets closer to 1, the slope becomes more unstable, and ultimately fails once the factor of safety drops below 1. There are many different geoenvironmental factors (i.e. slope angle, material composition, precipitation, etc.) that influence the balance between shear strength and shear stress and therefore ultimately determine the likelihood of slope failure.

Precipitation plays an important role in slope instability because it contributes to factors that can either increase shear stress and/or decrease shear strength. When it rains, water that falls on the Earth's surface will either infiltrate into the subsurface, be taken up and removed by evapotranspiration, or runoff into streams and rivers. Surface run-off leads to higher stream discharge which can physically destabilize a slope by eroding its underlying or lateral supports. Infiltration can raise the subsurface water level which increases the hydrostatic pressure between sediment particles. While some moisture can increase the ionic bonds between particles, once all of the pore spaces between particles are completely filled, additional moisture destroys those internal bonds and produces a fluid (Ritter et al., 2002).

Mass-Movement Classification

Mass movement types are classified into five distinct categories: slides, falls, flows, topples, and spreads (Cruden and Varnes, 1996; Hungr et al., 2014) [Figure 2]. Slides are further distinguished by the nature of the failure plane. Rotational slides have a concave rupture surface in which the head of the displaced material moves vertically downward, and the upper surface tilts back toward the scarp. Translational slides are generally shallower than rotational failures and occur on planar surfaces such as faults, joints, bedding surfaces, or contacts between soil and underlying parent material. Flows

are rapid forms of mass movement that mobilize saturated loose soil or rock on steep slopes and behave as viscous fluids. Falls are abrupt downward movements of rock or earth that detach with little or no shear displacement and descend from steep slopes or cliffs. Topples result from a similar detachment process as falls, though the material also experiences a forward rotation around an axis below its center of gravity. Spreads are commonly associated with seismic activity and usually occur on very gradual, nearly flat, slopes from the extension of one layer over another layer of differing rigidity. When two or more of these processes occur congruently, the movement type is classified as "complex" (Highland and Brobowsky, 2008). Material type is also considered during classification to distinguish between mass-movements of rock, debris, or earth [Figure 2].

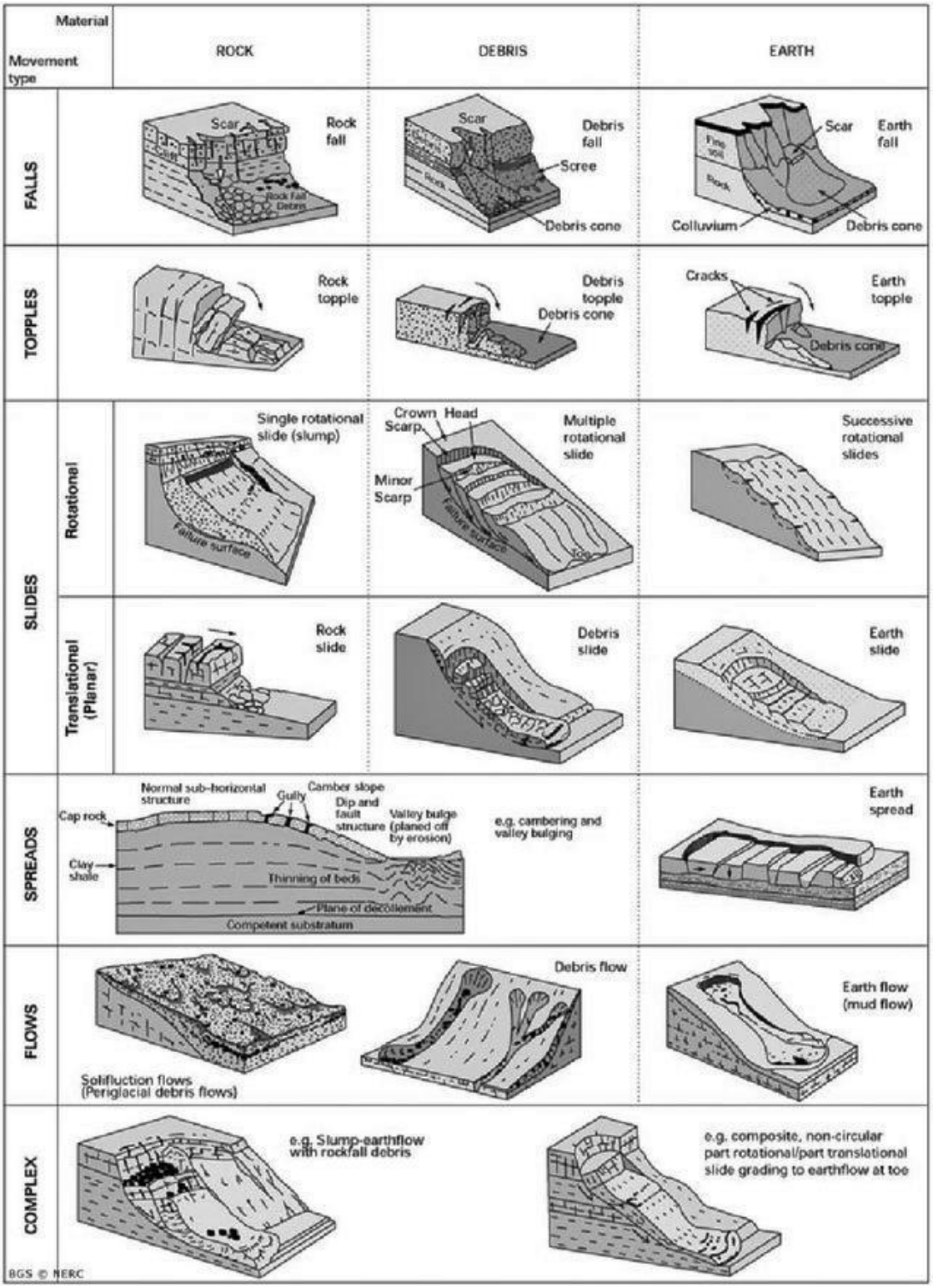

Figure 2. Landslide classification system by the British Geological Survey based on Varnes (1978) and Cruden & Varnes (1996).

Landslide Inventory Mapping

The first step in assessing landslide hazards is identifying active or historically-active slide areas to create an inventory of where slope failures occur. A typical landslide inventory contains information about the movement type, magnitude, date, and place of occurrence (Martha et al., 2010). Geomorphological landslide inventories are mapped using physical features of the landscape to identify landslides through visual interpretation of aerial photographs, satellite imagery, high-resolution Digital Elevation Models (DEMs), field mapping, or a combination of multiple mapping techniques. Regardless of the mapping method, all approaches operate under a few essential assumptions. First, landslides leave discernible signatures or scars in the landscape that can be recognized, classified, and mapped. Trained geomorphologists can distinguish these features in the field or through careful interpretation of high-resolution aerial imagery or digital representations of surface topography (Guzzetti et al., 1999). Second, landslides are not random occurrences but are instead the result of the interaction of physical processes governed by physical laws that produce different discernable morphologies (Guzzetti et al., 2012). Third, landslide morphology is dependent on the type of movement and rate at which the slope failure occurs. Essentially, similar types of mass movements produce similar morphological signatures (Guzzetti et al., 2012).

Despite these assumptions, the quality of an analysis is often dependent on the quality of the landslide inventory and the resolution of the spatial data used to build it. Fortunately, the increasing availability of high-resolution spatial topographic data and GIS capabilities allows geologists to successfully map and assess landslide hazards remotely (Crawford, 2012; Jaboyedoff et al., 2012). Landslide mapping is an evolving field, and geomorphologists are constantly exploring new methodologies and technologies to map landslides over large areas. Disparities in mapping methods can lead to variation in quality and inconsistent results, so standardized protocols for landslide mapping using lidar in GIS have been established by Oregon and Washington State (Burns and Madin, 2009; Slaughter et al., 2017). These standards produce landslide inventories that can be compared and effectively utilized in statistical landslide susceptibility models. As long as an inventory meets the standard protocols, does not underestimate specific landslide types, and has no significant geographical biases with

some areas covered more accurately or completely than other areas, it can be an effective tool for susceptibility analysis (Reichenbach et al., 2018).

Susceptibility Analysis

Future slope failures are more likely to occur under the same conditions that led to past instability. Therefore, information obtained on existing or historical landslides in an area can be generalized and used to detect landslides in other similar areas in the form of a susceptibility map (Guzzetti et al., 2012). Statistically-based landslide susceptibility models quantitatively analyze the relationships between instability factors and the distribution of landslides.

Published susceptibility assessments use various statistical models and their methodologies are constantly changing as statistical software evolves. A critical review of statistically based approaches to landslide susceptibility modeling identified 163 unique model type names out of 565 peer-reviewed articles published from 1983 to 2016 (Reichenbach et al., 2018). There is concern that experimentation with new or different statistical methods has overshadowed the relevant task of obtaining reliable susceptibility assessments, further complicating the comparison of susceptibility models (Reichenbach et al., 2018).

The four most common statistical methods are logistic regression, data overlay, neural networks, and index-based models (Budimir et al., 2015; Reichenbach et al., 2018). Multivariate logistic regression models are the most popular statistical methods and are shown to be the most reliable in several comparative studies (Aleotti and Chowdhury, 1999; Guzzetti et al., 1999; Lee and Sambath, 2006; Guzzetti et al., 2006; Yilmaz, 2010; Mancini et al., 2010; Ozdemir and Altural, 2013).

The multiple logistic regression analysis predicts the probability of a binary dependent variable (landslide occurrence) using a set of independent predictor variables (geoenvironmental factors). The regression accommodates the binary outcome by fitting a sigmoid curve using the logit function [Figure 3].

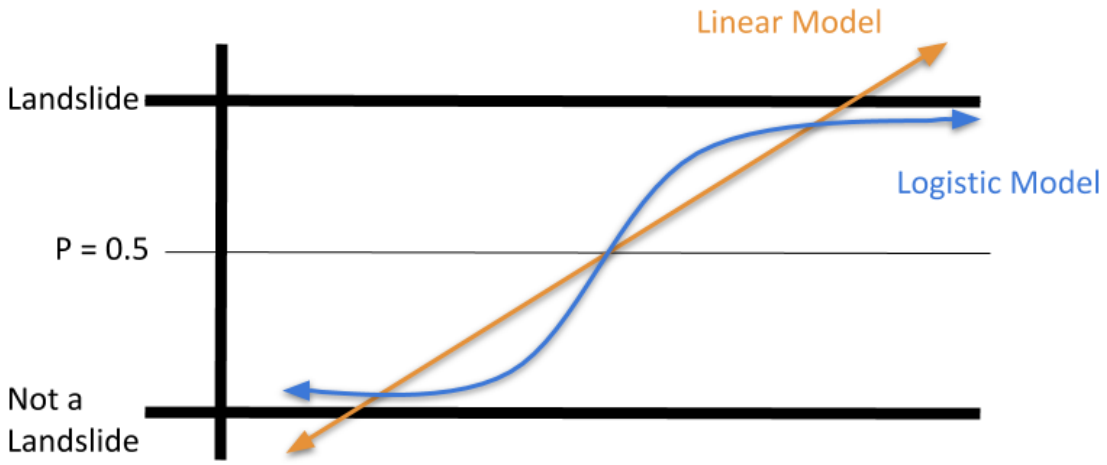

Figure 3: Comparing linear regression to Logistic regression.

The *logit* is the natural log of the odds:

$$\log(\text{odds}) = \ln\left(\frac{P}{1-P}\right) = \beta_0 + \beta_1 x_1 \qquad (2)$$

Where the log of the odds is a function of the probability (P), β_0 is the intercept, β_1 is the coefficient, and x_1 is the variable.

$$\frac{P}{1-P} = e^{\beta_0 + \beta_1 x_1} \qquad (3)$$

$$\mathrm{P} = \frac{e^{\beta_0 + \beta_1 x_1}}{1 + e^{\beta_0 + \beta_1 x_1}} = \frac{1}{1 + e^{-(\beta_0 + \beta_1 x_1)}} \qquad (4)$$

Terrain slope has proven to be the single most effective variable used for susceptibility modeling while aspect, elevation, and curvature are less justified and may be controlled by local conditions (Fabbri et al. 2003; Budimir et al. 2015). For example, Fabbri et al. (2003) demonstrated that the performance of a susceptibility model using elevation, aspect, and slope performed significantly better than a model using bedrock geology, surficial deposits, and land use in Belgium and Portugal case studies. The

success of a logistic regression susceptibility analysis depends on the quality and relevance of the information used to construct it.

Study Area

Northeastern Minnesota is a dynamic landscape with a unique geologic history of tectonics and continental glaciation that continues to influence modern geomorphology. Because slope stability is affected by the topography, geology, and climate of the region, we must establish a solid understanding of the local climate trends, bedrock geology, glacial history, and postglacial isostatic adjustment.

Bedrock Geology

The bedrock geology of this region primarily consists of stacked basalt flows and gabbroic igneous intrusions that formed approximately 1.1 Ga (billion years ago) during a failed mid-continental rift system (Sims and Morey, 1972). The Duluth Complex gabbro, as well as other felsic and mafic extrusive rocks that comprise the North Shore Volcanic Group, are exposed in outcrops of steep rocky bluffs along the shoreline of Lake Superior. The Fond du Lac Formation (~1.0 Ga), which can be found southwest of Duluth, contains sedimentary bedrock composed of weak sandstone, siltstone, and inter-bedded shale (Morey, 1967; Finley-Blasi, 2006). Even further south, tilted greywacke sandstone and siltstone beds of the Thompson Formation (~1.8 Ga) outcrop where the St. Louis River cuts through Jay Cooke State Park in Carlton County (Ojakangas and Matsch, 1982).

Surficial Geology

The surficial geology of the North Shore of Lake Superior reflects the incredible geomorphic power of glaciation. During the Wisconsin glaciation, massive ice lobes on the margins of the Laurentide ice sheet advanced and retreated several times shaping the surficial geology and topography. Four main phases of glacial advance occurred during the late-Wisconsin, in which three main ice lobes (Superior, Rainy, and sub lobes of the Des Moines) were responsible for eroding and redistributing sediments throughout the

area [Figure 4]. Each successive advance covered a smaller area, depositing finer-grained till from pro-glacial lake sediments that were re-incorporated into the ice (Hobbs et al., 2011). Pro-glacial lakes formed from meltwater that accumulated behind moraines, which acted as dams while the Superior lobe retreated to the northeast. These pro-glacial lakes coalesced to form glacial Lake Duluth roughly 11,000 calibrated calendar years before present (Breckenridge, 2013). Paleo-lake levels can be recognized by a combination of geomorphic features such as terraces, beach ridges, spits, tombolos, wave-cut cliffs and deltas. Shoreline features from glacial Lake Duluth are present in a thin band inland of the southwest margin of Lake Superior (Leverett, 1929; Hobbs, 2004; Breckenridge, 2013).

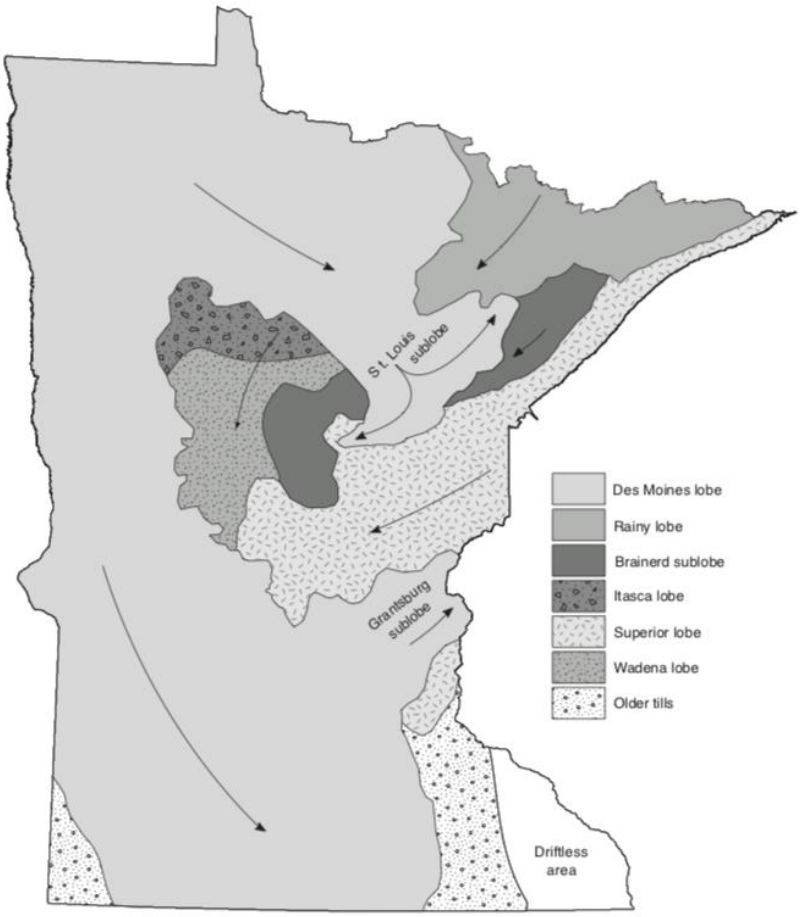

Figure 4. Simplified map depicting flow direction and extent of ice lobes that covered Minnesota during the Wisconsin glaciation (Lusardi and Dengler, 2017).

Two distinct glacial till formations deposited along the North Shore by the Superior Lobe during the late-Wisconsin glaciation can be distinguished based on their color, texture, and composition. The Cromwell formation is described as a reddish-brown loam matrix that contains a range of 1- 45% coarse-grained fragments of primarily igneous rocks including basalt, rhyolite, diabase, and gabbro from the northeast (Hobbs, 2003; Hobbs, 2004). The Barnum formation is a clayey till that overlies the Cromwell formation and is further distinguished by three member units (Hobbs et al., 2011). The Lakewood member sits above the Cromwell Formation and is a reddish-brown silty loam with about 6-12% coarse-grained fragments (Hobbs, 2003; Hobbs, 2004). The second unit is the Moose Lake member, a reddish-brown silty clay loam with approximately 3-6% coarse-grained fragments (Hobbs, 2004). There is also a lacustrine silt and clay member, which sits on top of the Moose Lake member, known as the Wrenshall Formation that is laminated with red and grey varve sequences (Hobbs et al., 2011). The top unit is the Knife River member, a reddish-brown clay that contains 1-3% coarse-grained fragments (Hobbs, 2004). These tills and lacustrine deposits are composed of 40-100% silt and clay and demonstrate a general fining-upward trend.

By approximately 11,000 years ago, Minnesota was mostly ice-free except for the Rainy lobe, which still covered some area in the farthest northeastern portion of the state [Figure 4]. The Rainy lobe deposited a brown, sandy till containing basalt, gabbro, and other igneous and metamorphic rock fragments sourced from the Canadian Shield (Lusardi and Dengler, 2017).

Isostatic Adjustment & Landscape Morphology

Isostatic rebound and knickpoint migration in response to base level changes are significant impacts of glaciation that continue to affect regional geomorphology. Historical changes in glacial lake levels initiated knickpoint migration and channel incision within all tributaries to Lake Superior. Anthropogenic land use and forest clearing, in addition to natural base level changes, have exacerbated the level of erosion in these incised systems for most sub-basins of the Lake Superior watershed. Crustal uplift from isostatic rebound in this region is faster to the northeast where ice sheets were thickest; therefore, the land surface is tipping with greater uplift in the north forcing

water towards the southwest shore of Lake Superior (Lee and Southam, 1994). This isostatic adjustment causes a gradual drop in base level to the northeast and a rise in base level to the southwest. Rising base level increases coastal erosion while base level drop leads to knickpoint migration and channel incision. Channel incision through glacial till produces significant stream bank scour and slumping, contributing abundant fine sediments into local streams (Wick, 2013; Neitzel, 2014; Hall, 2016; Jasperson et al., 2018).

Climate Trends & Implications

Climate and precipitation are known to influence slope stability and trigger mass movement events (Cruden and Varnes, 1996; Crozier, 2010). Changes to these factors can potentially impact the frequency and severity of landslide activity in a region. As global climate change continues, regional impacts reveal themselves. Climate trends over the past several decades in Minnesota show an increase in annual precipitation with more frequent heavy rainfall events (Blumenfeld, 2016). These trends are projected to continue according to several climate change scenarios (Handler et al., 2014). Modeling studies conducted with differing sensitivity to emissions scenarios present two model projection results; Geophysical Fluid Dynamics Laboratory (GFDL A1FI) by the National Oceanic and Atmospheric Administration (NOAA) and Parallel Climate Model (PCM B1) by the National Center for Atmospheric Research (IPCC, 2007). Although both projections are possible, the GFDL A1FI scenario represents a more realistic projection of future greenhouse gas emissions and temperature increases (Raupach et al., 2007). Increasing precipitation could have implications for slope stability and erosion in the Lake Superior watershed, further emphasizing the need for this type of research.

Northern Minnesota has already experienced a climate that is relatively "warmer" and "wetter" than previous decades (Blumenfeld, 2016). Mean annual temperature increased 1.2 °C (2.2 °F) from 1901 to 2011 and the North Shore of Lake Superior has warmed faster than surrounding areas during winter months (Handler et al., 2014). Warmer winter air temperatures have led to more snowmelt in intervening periods between snowfall events. During the entire 20th century, there appears to have been a 12 to 22-day decline in the annual number of soil frost days (Sinha et al., 2010). Mean

annual precipitation increased by 5.8 cm (2.3 in) across the entire assessment area (Handler et al., 2014). In addition to an increase in annual precipitation, the frequency of intense precipitation events has also increased across Minnesota. A 102% increase was observed in rainstorms of 7.6 cm (3 in) or more between 1920 and 2011 (Saunders et al., 2012).

Northern Minnesota is projected to experience profound changes in regional climate by the end of the 21st century; including shifts in mean temperature and precipitation with altered timing and intensity (Handler et al., 2014). Compared to the baseline period (1971-2000), the average annual temperature is projected to increase 1.7 °C (3.0 °F) under the PCM B1 scenario and 4.9 °C (8.8 °F) under the GFDL A1FI scenario. The PCM B1 scenario projects that Northern Minnesota will receive on average 7.6 cm (3 in) more annual rainfall at the end of the next century compared to the baseline period. However, the GFDL A1F1 scenario projects that Northern Minnesota may experience a slight decrease in annual rainfall during this same period (-0.1 cm; -0.4 inches), with a larger decrease occurring during summer months (Handler et al. 2014). Rainfall from high-intensity events represents a larger proportion of the total annual and seasonal rainfall, which suggests the precipitation regime is becoming more episodic. An assessment covering the entire Great Lakes region projected that the frequency of single-day and multi-day heavy rainfall events could double by 2100 (Kling et al., 2003). Both climate models project changes that affect several hydrologic drivers for slope failures (i.e., precipitation, flooding, stream power, wave action, etc.), which could have implications for future frequency or severity of mass movement events.

On June 19th-20th of 2012, a record storm event released 20-25 centimeters of rainfall over 48 hours in Duluth, MN and surrounding areas, following one of the wettest Mays in Duluth's recorded history (Czuba et al., 2012) [Figure 5]. Extensive flooding triggered hundreds of mass-wasting events that damaged local infrastructure and contributed large volumes of sediment into tributaries of Lake Superior (Fitzpatrick et al., 2016). Since the 2012 storm event was well-documented and the landscape response was captured in repeat high-resolution lidar, these impacted areas serve as an ideal case study for how large storms trigger slope failures in similar postglacial landscapes.

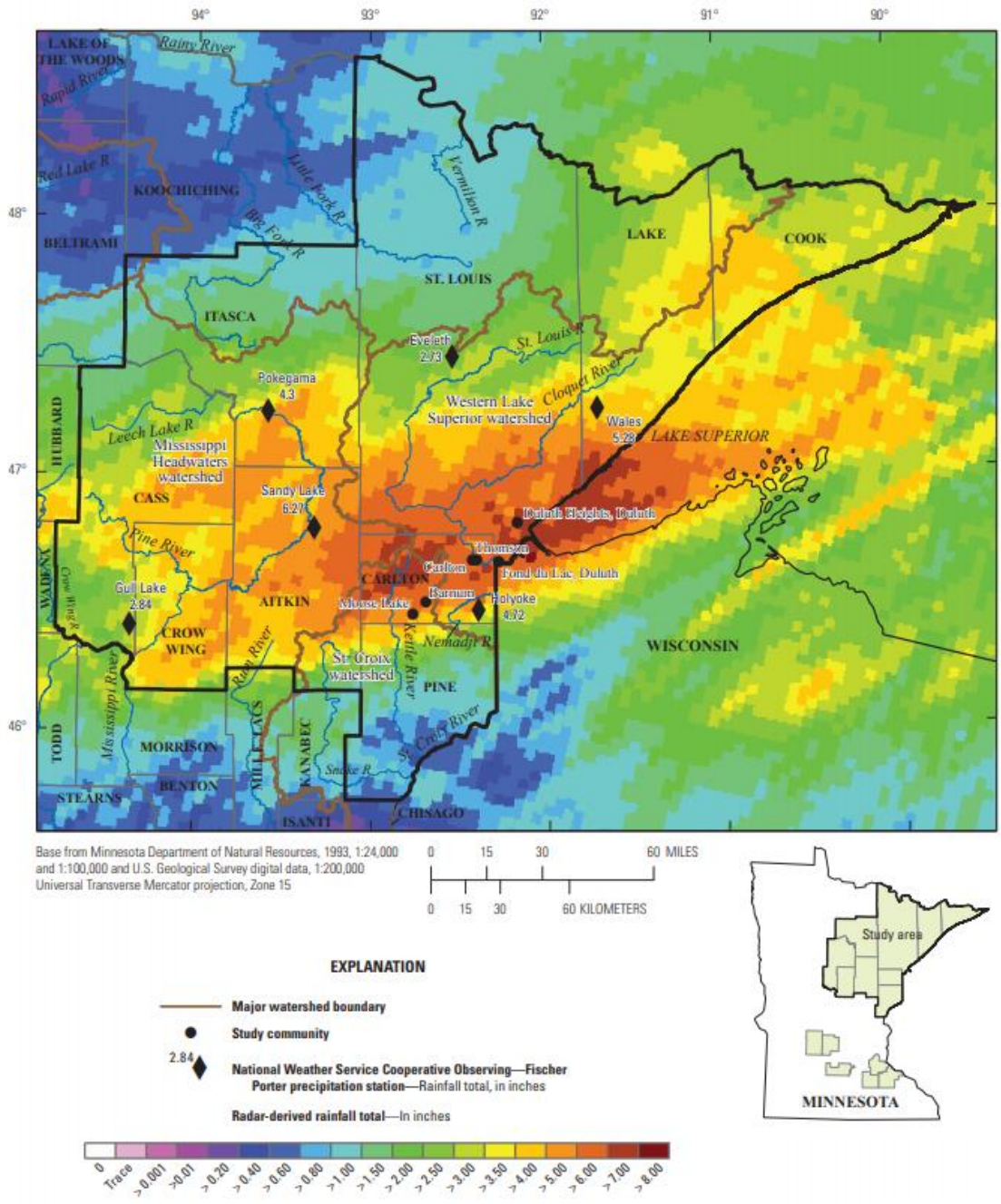

Figure 5. USGS report figure showing the distribution of rainfall across northeastern Minnesota from June 19 - June 21, 2012, using rainfall data from select National Weather Service (NWS) precipitation stations (Czuba et al., 2012).

Focus Areas

Landslide inventory mapping was completed for the entire Lake Superior Watershed in Minnesota with the exception of active mining areas [Figure 8]. Three subsections of the watershed serve as optimal case studies for landslide susceptibility because they represent different glacial settings: Jay Cooke State Park (JCSP), Lake Superior South watershed (LSSW), and the Mission Creek watershed (MCW) [Figure 6]. These three study areas were also similarly impacted by a major rainfall event in 2012 that triggered hundreds of landslides.

One area that was hit particularly hard in terms of erosion during the 2012 storm was Jay Cooke State Park. The park is 32.8 square kilometers of mixed forests, shrubs, and wetlands growing in clay-rich soils on top of glaciolacustrine sediments that have been carved down to bedrock by the St. Louis River and its tributaries. The underlying bedrock is primarily slate and greywacke of the Thompson Formation overlain with red

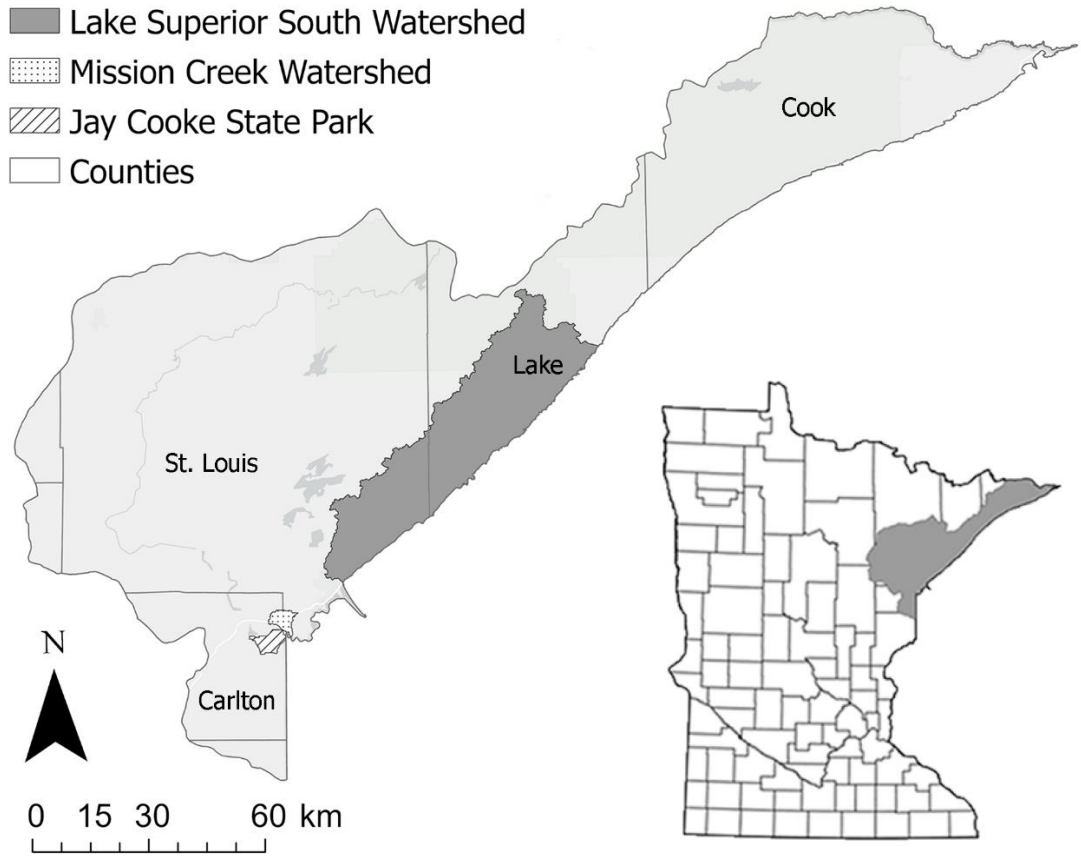

Figure 6. Map of the Lake Superior watershed in Minnesota, depicting study areas for susceptibility analysis.

clay and silt that settled out in the glacial Lake Duluth basin over 10,000 years ago. The 2012 flood washed out roads and caused larger landslides along highway 210 in Jay Cooke State Park which took five years and $21.3 million to repair (Kraker, 2017).

The nearby Mission Creek watershed is 28.5 square kilometers of mostly forest and grassland with a small percentage of rural development. Mission Creek is a tributary to the St. Louis River and its outlet is located near the neighborhood of Fond du Lac in southwest Duluth, just northeast of Jay Cooke State Park. Unlike most of the North Shore, the bedrock in this area consists of stacked sandstones and shales. This area has complex surficial geology because of its location on the paleo-shoreline of glacial Lake Duluth. The area thus contains a combination of glacial outwash deposits and glaciolacustrine sediments containing high concentrations of fine sand, silt, and clay. Mission Creek experienced similar destabilization in 2012 from intense rainfall and flooding.

The Lake Superior South watershed is 1,628 square kilometers within the Lake Superior watershed. This watershed covers a variety of urban, suburban, and rural residential areas in addition to mixed forested and wetland areas. This watershed represents an ice-marginal glacial setting in which most of the unconsolidated glacial material belongs to the Cromwell or Barnum formations deposited in the Highland and Nickerson ground moraines.

Variation in the underlying geology across northeastern Minnesota could explain trends in the frequency and distribution of slope failures as well as the different types of failures that occur. The diverse geology across the region also presents a challenge for modeling landslide susceptibility.

Methods

Historic Inventory

Previously documented locations where mass movements have occurred are considered historic landslides and were compiled into a historic inventory (Jennings et al., 2016). Online newspaper archives and articles allowed us to locate several mass

movement events documented by the media (e.g., Star Tribune, 2011; Pine journal, 2011; Duluth News Tribune, 2012; Twin Cities Pioneer Press, 2015). A database of GPS-referenced photos taken by volunteers after the 2012 flood event, identifying areas of erosion and flood damage, were valuable event-based landslides incorporated in the historic inventory (B. Frederickson, MPCA, personal communication). Local and state agencies like the South St. Louis and Lake County Soil and Water Conservation District (SWCD) shared sites of erosion on private property reported by landowners (D. Passe, Lake Co., personal communication, 2018). Datasets received from completed master's thesis research on bluff erosion (Wick, 2013; Neitzel, 2014; Manopkawee, 2015; Hall, 2016), sediment stressor reports (Jasperson et al., 2018; Lahti et al., 2013; Sandberg et al., 2017), and river basin studies (Natural Resource Conservation Service, 1998; St. Louis SWCD, 2010; Nieber et al., 2008) were also included in the historic inventory database [Appendix 1: Figure 15].

Historical imagery (1991-2019) and three-dimensional perspectives on Google Earth were used to identify potential historic landslide locations remotely. Landslide scars and deposit signatures (i.e., bare earth, breaks in the tree canopy, clusters of fallen trees, etc.) were identified remotely using Google Earth imagery. We remotely surveyed along main-stem river corridors, major roads, highways, and the shoreline of Lake Superior. Location confidence was rated using a 3-point scale based on the type of data collection methods used. Site locations provided by external sources are considered "potential erosion locations" and rated with low confidence "1". Any potential locations that were verified using Google Earth imagery were rated with moderate confidence "2". Field-verified locations were given the highest confidence rating "3". Each site in the historic inventory was assigned a confidence rating and any available information was included in a table of attributes [Appendix 2: Table 13].

Remote Mapping

Following guidelines provided by Oregon and Washington State protocols for mapping landslides from airborne lidar data (Burns and Madin, 2009; Slaughter et al., 2017), all historic landslide locations were digitized into polygon feature classes that distinguish between the failure's "headscarp", "deposit", and additional "scarp line"

features. All feature classes were incorporated into a landslide geodatabase adapted from Oregon and Washington's published geodatabase schema (Burns and Madin, 2009; Slaughter et al., 2017) and customized for Minnesota (Engle et al., 2020). One-meter digital elevation models (DEMs) produced from airborne lidar flights were used to generate detailed visualizations of the topography (i.e., hillshade, slopeshade, and Red Relief) which help illuminate landslide features in ArcGIS (ArcMap & ArcGIS Pro) [Figure 7]. Slopeshade refers to a slope map displayed with a red-to-white color ramp using a stretched symbology with 5 standard deviations. Red Relief [Figure 7b] is a topographic visualization built by layering a 40% transparent slopeshade over a raster known as “topographic openness” (Yokoyama et al., 2002; Chiba et al., 2008).

Airborne lidar flight missions were conducted in 2011 (pre-flood) and 2012 (post-flood) in Carlton and St. Louis Counties. Repeat aerial lidar typically allows for vertical change detection that reveals areas of erosion and deposition. Unfortunately, errors in the Duluth-area lidar alignment inhibited an accurate assessment of net volumetric changes. Horizontal and vertical offsets found in the lidar data were caused by different flight line directions and misalignments. USGS is currently working to remediate these misalignments and explore new ways to utilize the data with Object-Based Image Analysis (OBIA) for landslide detection (DeLong et al., 2020). High-resolution aerial imagery from 2013 was sourced from the National Agriculture Imagery Program (NAIP) and accessed through the Minnesota IT Services Geospatial Information Office to guide mapping in ArcGIS. Google Earth imagery from 2015 and 2017 was also referenced often throughout the mapping process.

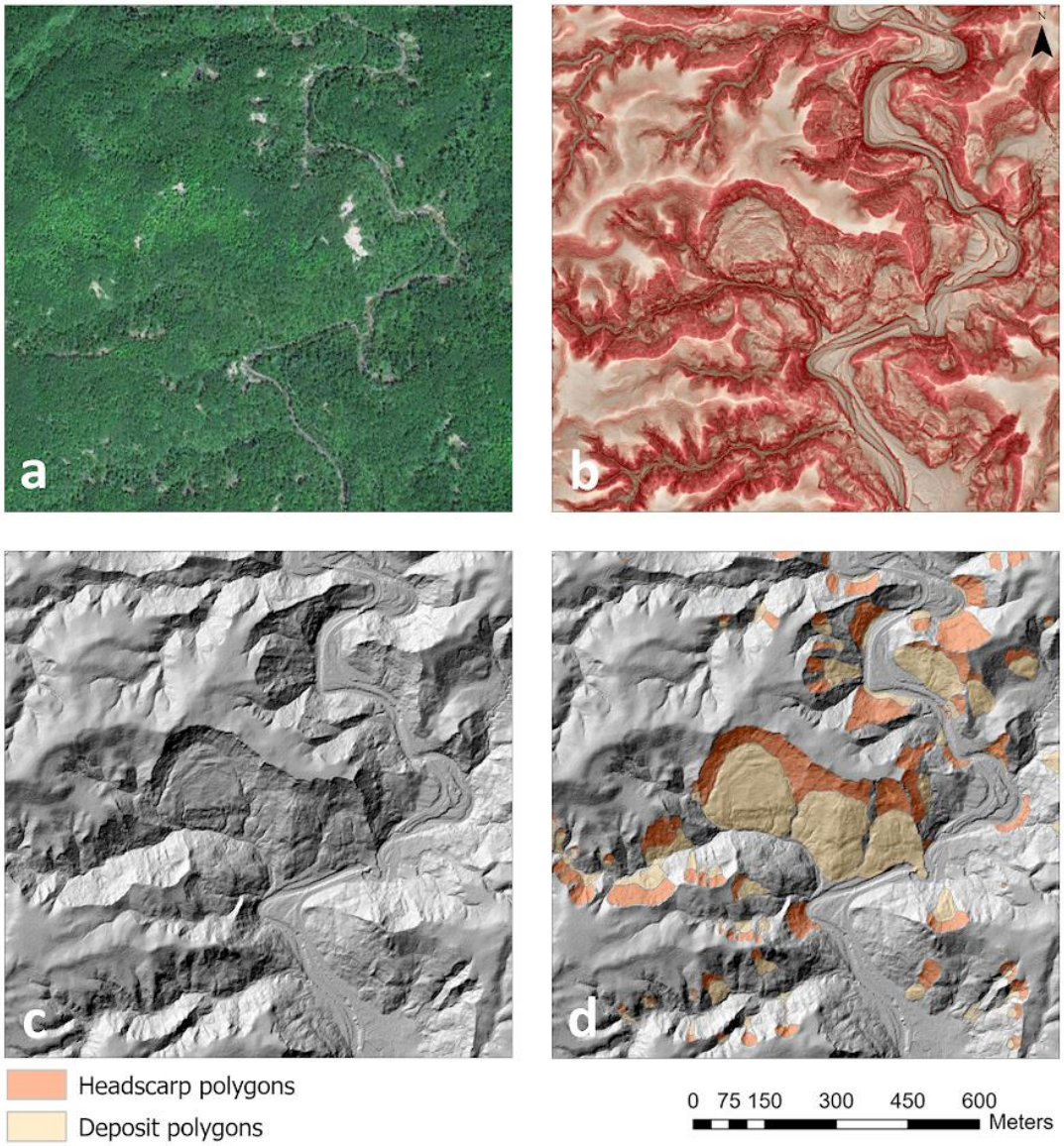

Figure 7. Aerial imagery (a), Red Relief (b), and lidar hillshade (c) were used to delineate landslide polygons (d).

Mapping was conducted at a map scale ranging from 1:1000 - 1:3000. The editor tool was used to outline headscarps and deposits separately using three primary data visualizations as base maps: aerial imagery, Red Relief, and 1-meter lidar hillshade [Figure 6]. Each headscarp polygon includes a headscarp feature and/or exposed failure surface. Headscarp and associated deposit polygons were given matching slide unique id numbers. In the case where a headscarp contributes to multiple deposits, the first mapped deposit was given a matching slide unique id and remaining deposits were numbered

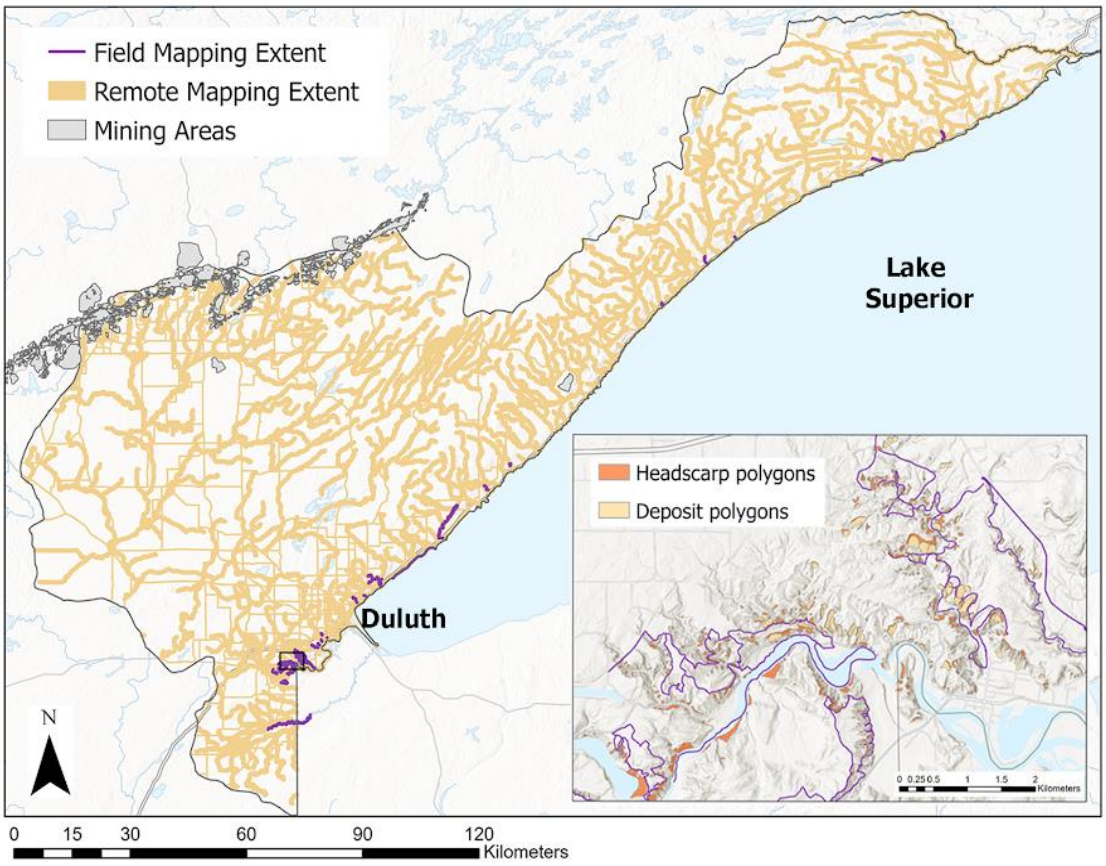

Figure 8. Remotely mapped extent, field-verified areas and excluded mining areas. Inset map shows landslide polygons and the purple lines depict paths taken by researchers during field-verification of the Jay Cooke State Park area.

consecutively. In many cases, deposited material was removed by streams, rivers, or waves, and therefore showed no evidence of a mappable deposit. Information about the mapped slides (e.g. location method, confidence, slope, aspect, material, etc.) was included in a slide properties table as part of the geodatabase [Appendix 2: Table 14].

Field Verification

Field verification was used to validate and assess remote mapping methods as well as provide additional field data and observations. We selected areas to field-check that were easily accessible and had high landslide density. We utilized public hiking trails and walkable streams to access many of our sites [Figure 8]. Areas along larger water bodies were accessed via canoe or small fishing boat. We tracked our field exploration

using a Garmin InReach hand-held GPS unit. Trimble GNSS units with laser rangefinders were used to collect multiple offset GPS points per site. At each slide, we collected GPS points for the headscarp feature, flanks, deposit (if present), and photo locations. Base maps containing our mapped polygons were uploaded to the Trimble for efficient on-site location and to report any missing or inaccurate polygons. Photos were taken at each site and included in the landslide geodatabase. Field notes for each site included a description of slide material, slide classification, estimated headscarp height, photo time stamp, and any additional observations on slope failure processes. Sediment samples were collected at select sites using a hand shovel and labeled quart size bag to confirm material descriptions back in the lab.

Susceptibility Analysis

I conducted a susceptibility analysis using a logistic regression (LR) approach to predict the landslide occurrence using nine causal factors: (slope, aspect, elevation, relief, depth to bedrock, soil erodibility, substrate, land cover, and distance to streams). This LR analysis was tested in Jay Cooke State Park (JCSP) and the Lake Superior South watershed (LSSW) to compare changes in model performance at different spatial scales and geomorphic settings. The two predictive models were then applied to the Mission Creek watershed to assess the impact of scale and setting on transferability.

Pre-flood (2011) 1-meter digital elevation models (DEMs) were used for all raster derivations in the susceptibility analysis. Slope and aspect were generated using their respective tools in ArcGIS. Aspect was reclassified into a factor with each cardinal direction as a separate class. Local relief was created using the focal statistics tool to calculate the range (maximum-minimum) of nearby pixel values using a 100m x100m moving window. The distance to stream raster was created using the Euclidean distance tool to calculate distance from the statewide Department of Natural Resources (DNR) streams and rivers shapefile. The depth to bedrock raster dataset was sourced from the Minnesota Geological Survey (MGS) County Atlas.

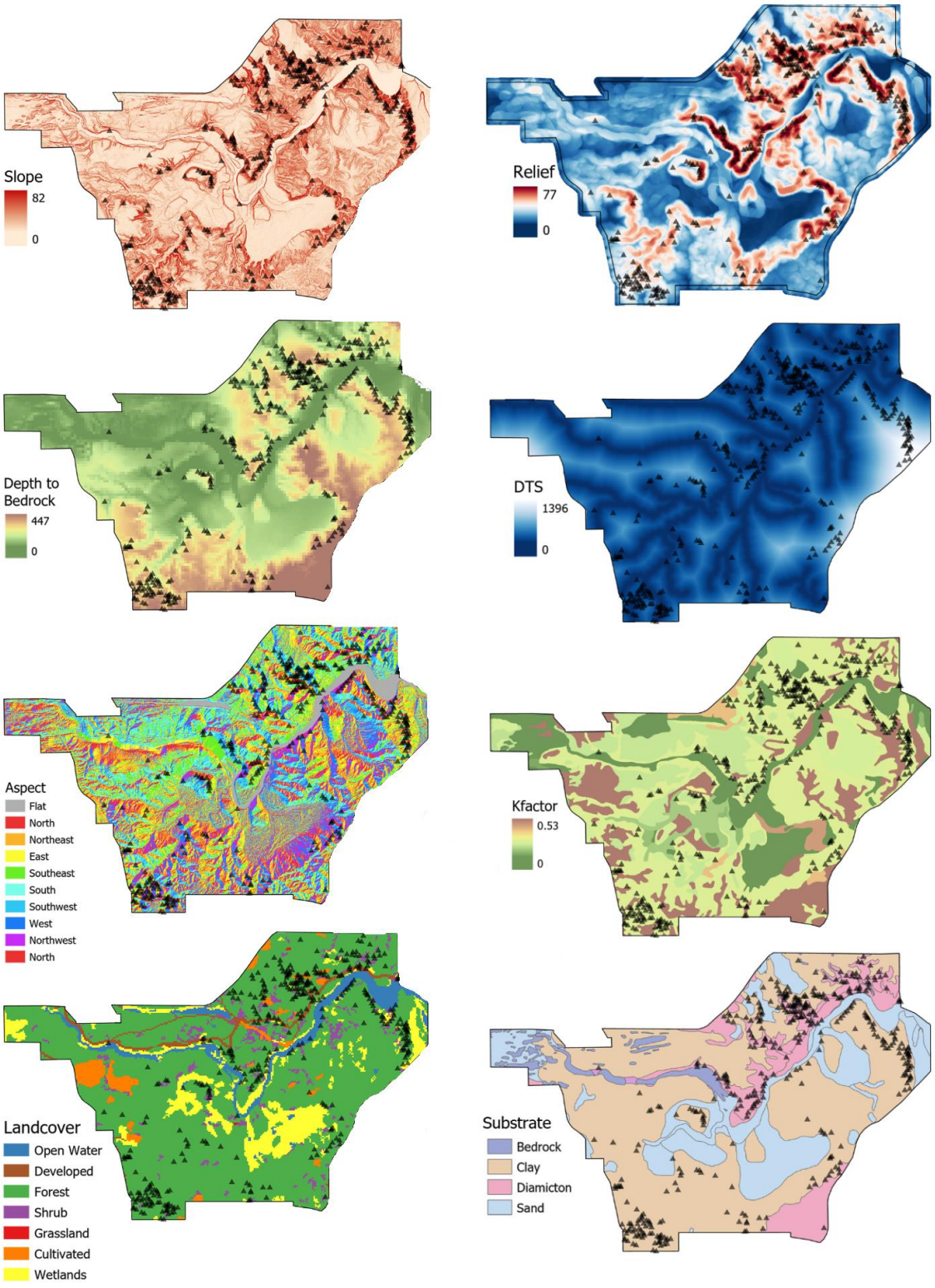

Figure 9. Predictive variables included in the analysis: Slope (a), Relief (b), Depth to Bedrock (c), Distance to Streams (d), Aspect (e), K-factor (f), Landcover (g), and Substrate (h).

Land cover data from 2011 came from the National Land Cover Dataset (NLCD) and was reclassified into 8 categories. Surficial geology data sourced from the MGS was converted from a shapefile to a raster layer using the "lithology" attribute to assign individual pixel values. Bedrock geology was converted from a shapefile to a raster with the "Major lithology" attribute assigned to individual pixels. Soil erodibility from the Soil Survey Geographic database (SSURGO) was converted from a shapefile to a raster dataset using the "k-factor" attributes assigned to pixels. Land cover, depth to bedrock, and distance to stream were resampled to match DEM derivative rasters (1m x 1m cell size) to maintain the highest possible resolution. [Appendix 3]

For the logistic regression analysis, geoenvironmental information is required for landslide areas and non-landslide areas. To collect a balanced sampling of points for "stable" non-landslide areas, we created a fishnet of points across the area of interest and

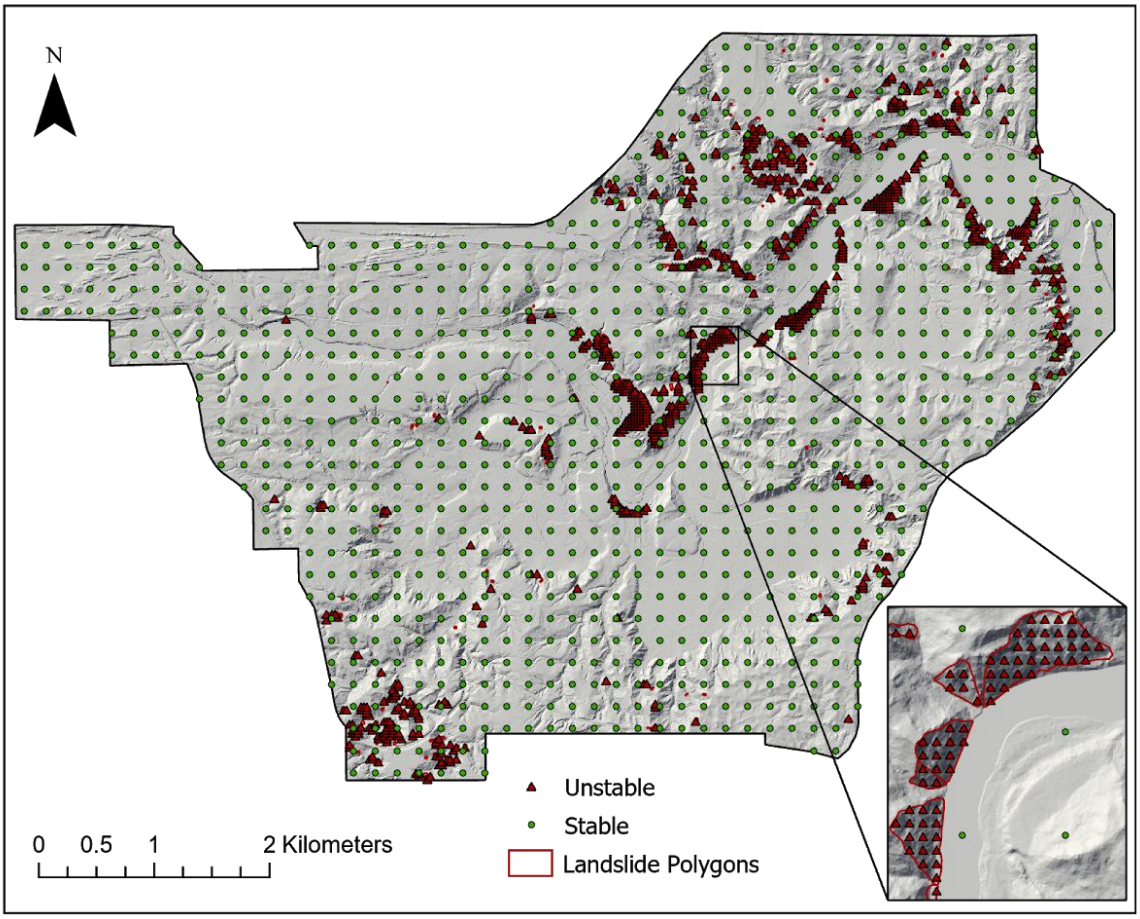

Figure 10. Map depicting data sampling in stable and unstable areas of Jay Cooke State Park.

used "extract multi values to points" to sample pixel values from the raster. A similar technique was used to sample "unstable" landslide areas using a denser fishnet of points across landslide polygons [Figure 10]. Any non-slide points overlapping with slide polygons were erased from the sampling. These data tables were exported to excel and arranged in a comma-separated values (.csv) format for use in R open-source statistical software (R Core Team, 2019). We randomly subdivided the dataset into 80% training data and 20% test data for cross-validation.

The Generalized Linear Model (glm) function was used to run a multivariate Logistic Regression (LR) in R statistical programming software (R Core Team, 2019). Independent variables included non-linear, non-normally distributed, categorical data (substrate, land cover, and aspect), and continuous data (slope angle, relief, elevation, soil k-factor, depth to bedrock, and distance to streams). A correlation matrix was generated to identify any correlation between variables that would bias the LR model. Relief was eliminated because of its high correlation with slope. The glm was specified as a binomial because our dependent variable is binary (presence/absence of landslide). LR analysis of the training data evaluated the relative contribution of each variable, emphasizing variables with a statistically-significant influence on slope stability. We used the MASS package in R to apply a stepwise method in both directions that tests different combinations of variables (Venables and Ripley, 2002). The Akaike Information Criterion (AIC) is a common indicator for goodness-of-fit and is calculated using the log-likelihood and equivalent degrees of freedom (edf). In a glm, the log-likelihood represents the model deviance and the edf is determined by the number of parameters included in the model. AIC was used to compare models and identify which combination of predictive variables produced the best fitting model. Test data were utilized to determine how effectively the final model predicted landslide occurrence using a confusion matrix [Table 1]. A confusion matrix, or table comparing predicted values with actual test data values, was generated to assess model accuracy. Confusion matrices were also generated using spatial analysis in ArcGIS to show how accurately the external models predicted landslides in the Mission Creek watershed compared to the actual watershed inventory data.

Table 1. Confusion Matrix:

Actual	Predicted	
	Non-Slide	**Slide**
Non-Slide	True Negative	False Positive
Slide	False Negative	True Positive
Accuracy	**((TN + TP) / (Total)) * 100**	

Multiple iterations allowed us to manage variation that arose from randomly sampling training/test data and eliminate unnecessary predictive variables. Each iteration ran a simple LR using slope as the only predictive variable to compare with the multivariate LR analysis. We ran 1000 iterations and assessed how frequently each variable was considered significant by the model. Any variables that were included in less than 50% of the thousand iterations were excluded from the final analysis.

Once all variables were properly vetted, an additional 1000 iterations of the LR analysis were run to select our final susceptibility model. The variables included in the final analysis were slope, distance to streams, depth to bedrock, substrate, and k-factor. We selected the model with the lowest AIC or "best-fit" and used the model summary results to build a susceptibility map in ArcGIS. Each predictive variable raster was weighted based on its coefficient estimate using the raster calculator. The resulting landslide susceptibility raster was classified into three categories for low, moderate, and high susceptibility using ArcGIS Natural Breaks (Jenks). See appendix 3 for detailed instructions to replicate this analysis [Appendix 3].

Results

Landslide Inventory

The landslide inventory for the Lake Superior watershed in Minnesota contains 2,005 remotely mapped slope failures. During the 2019 field season, 685 out of 702 field-checked polygons were positively identified. The spatial distribution of these mapped

failures shows us that certain areas have a higher density of mass-wasting events. More than half of the inventory (52%) is located within Carlton County, St. Louis County contains almost a third of the inventory (31%), while the remainder is split between Lake (7%) and Cook (9%) counties.

The distribution of landslides is largely dictated by the surficial geology of the region. Over 70% of the mass movements occur in glacial sediments, with the majority in areas mapped as glaciolacustrine deposits of the Barnum formation and less than 3% of the mapped slides occur in areas mapped as diamicton from the Cromwell formation. 18% are found in areas mapped as Holocene alluvium. The remaining 10% of slope failures occur in bedrock members of the Duluth Complex and the North Shore Volcanic Group.

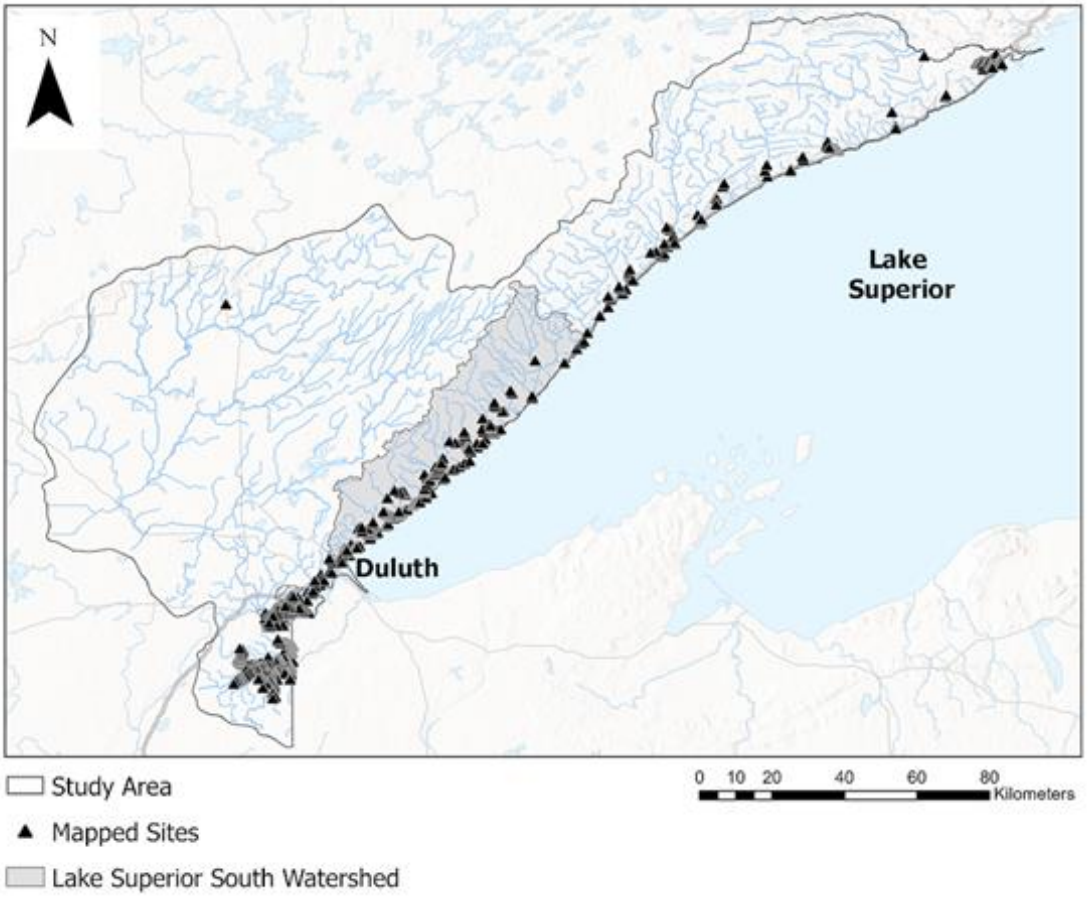

Figure 11. Landslide inventory for the Lake Superior watershed.

Table 2. Landslide inventory summaries for each focus area.

	# of Slides	*Area[*] (km^2)*	*Landslide Area (km^2)*	*Average[†] (m^2)*	*Minimum[†] (m^2)*	*Maximum[†] (m^2)*
LSW	2,005	15,699	2.6	1,306	11	40,304
LSSW	407	1,616	0.24	587	15	6,823
Jay Cooke	421	35	0.62	1,486	37	23,947
Mission Creek	266	28	0.31	1,177	24	13,777

[*] *Area of each watershed*
[†] *Average, minimum, and maximum polygon size in each watershed*

The most common types of mass movements we observe in northeastern Minnesota include shallow translational and rotational earth slides as well as complex slope failures. We identified shallow translational slides along sloped surfaces of stacked lithologies, at the interface of organic soils with underlying sediment (rooting depth), or where slopes have been modified to accommodate roads and other infrastructure. These translational failures often occur during freeze/thaw cycles or following periods of intense rainfall. Slumping, a form of rotational slope failure, is characteristic of most sediment bluffs along stream corridors of Lake Superior tributaries. These rotational failures result from increased soil moisture and undercutting of the bank's toe from direct hydraulic action (Hooke, 1979). Slumps can also result from the process of groundwater seepage or piping through the bank in a process known as "sapping" (Hagerty, 1991). Complex slope failures demonstrate morphologies for multiple movement types and commonly involve re-activation of a landslide deposit.

Less common mass-movement events include debris flows, earth flows, and rock falls/topples. Debris and earth flows occur in areas with high relief and thicker glaciolacustrine sediments or paleo-shoreline depositional environments. These are caused by intense surface water run-off from heavy precipitation or rapid snowmelt that saturate, liquefy, and mobilize unconsolidated fine-grained sediments (Highland and Bobrowsky, 2008). Rock falls and topples are typically found where streams and roads have cut down through bedrock and in the steep bedrock cliffs along the North Shore of Lake Superior. Rock falls are common in jointed bedrock and are triggered by

freeze/thaw, general physical and chemical weathering, or from direct undercutting from streams or wave action.

Susceptibility Analysis

The influence of slope on landslide occurrence is positively correlated with the slope angle. Logistic Regression (LR) analysis of slope stability in Jay Cooke State Park (JCSP) using slope angle as the only predictive variable with six slope categories predicted landslides with 81.4% accuracy. Landslide frequency gradually increases with an increase in slope angle and slopes of 32-45 degrees have the highest likelihood of failing in this area.

Table 3. Simple LR model summary results for Jay Cooke State Park:

	Estimate	**Std. Error**	**P-value**
(Intercept)	-5.02	0.71	<0.001
Slope (4-12)	1.71	0.78	0.03
Slope (12-23)	4.64	0.72	<0.001
Slope (23-27)	6.25	0.72	<0.001
Slope (27-32)	7.26	0.74	<0.001
Slope (32-45)	7.81	0.76	<0.001

Table 4. Confusion matrix for simple LR model in Jay Cooke State Park:

Actual	Predicted	
	Non-Slide	**Slide**
Non-Slide	203	35
Slide	52	180
Accuracy	**81.4%**	

The multivariate LR analysis of slope stability in JCSP indicated that slope, land-cover, substrate, depth to bedrock, and distance to streams are statistically significant (P < 0) variables for predicting the presence or absence of slope failures in JCSP. Slope was weighted more heavily in the model than land-cover, substrate, depth to bedrock, and distance to stream. The multivariate model predicted landslides with 82.3% accuracy.

Table 5. Multivariate LR model summary results for Jay Cooke State Park:

	Estimate	Std. Error	P-value
(Intercept)	-7.17	1.13	<0.001
Substrate (Clay)	-0.16	0.73	0.83
Substrate (Diamicton)	1.81	0.73	0.01
Substrate (Sand)	-1.08	0.81	0.19
Land cover (Developed)	0.76	0.73	0.30
Land cover (Forest)	0.85	0.56	0.13
Land cover (Open Water)	4.03	0.80	<0.001
Land cover (Shrub)	1.09	0.70	0.12
Land cover (Wetlands)	1.67	0.68	0.01
Depth to Bedrock (30-61)	0.80	0.37	0.03
Depth to Bedrock (61-96)	0.87	0.37	0.02
Depth to Bedrock (96-136)	0.80	0.36	0.03
Depth to Bedrock (136-187)	1.34	0.36	<0.001
Depth to Bedrock (187-413)	1.33	0.36	<0.001
DTS (52-82)	0.20	0.28	0.49
DTS (82-129)	0.00	0.27	1.00
DTS (129-201)	-0.07	0.27	0.80
DTS (201-312)	-0.62	0.29	0.04
DTS (312-1,370)	-0.62	0.29	0.03
Slope (2.6-4.3)	1.66	0.88	0.06
Slope (4.3-13.1)	4.52	0.81	<0.001
Slope (13.1-23.5)	6.15	0.82	<0.001
Slope (23.5-31.3)	7.19	0.83	<0.001

Slope (31.3-66.3)	7.74	0.86	<0.001

Table 6. Confusion matrix for multivariate LR model in Jay Cooke State Park:

Actual	Predicted	
	Non-Slide	**Slide**
Non-Slide	195	23
Slide	60	192
Accuracy	**82.3%**	

LR analysis of slope stability in the Lake Superior South watershed (LSSW) using slope angle as the only predictive variable with six geometrically binned slope categories predicted landslides with 95.2% accuracy. Relatively flat slopes (2.6-4.3 degrees) have a strong influence on slope stability while moderately steep slopes (31.5-66.3 degrees) have the largest likelihood of slope failure. High standard error and p-values associated

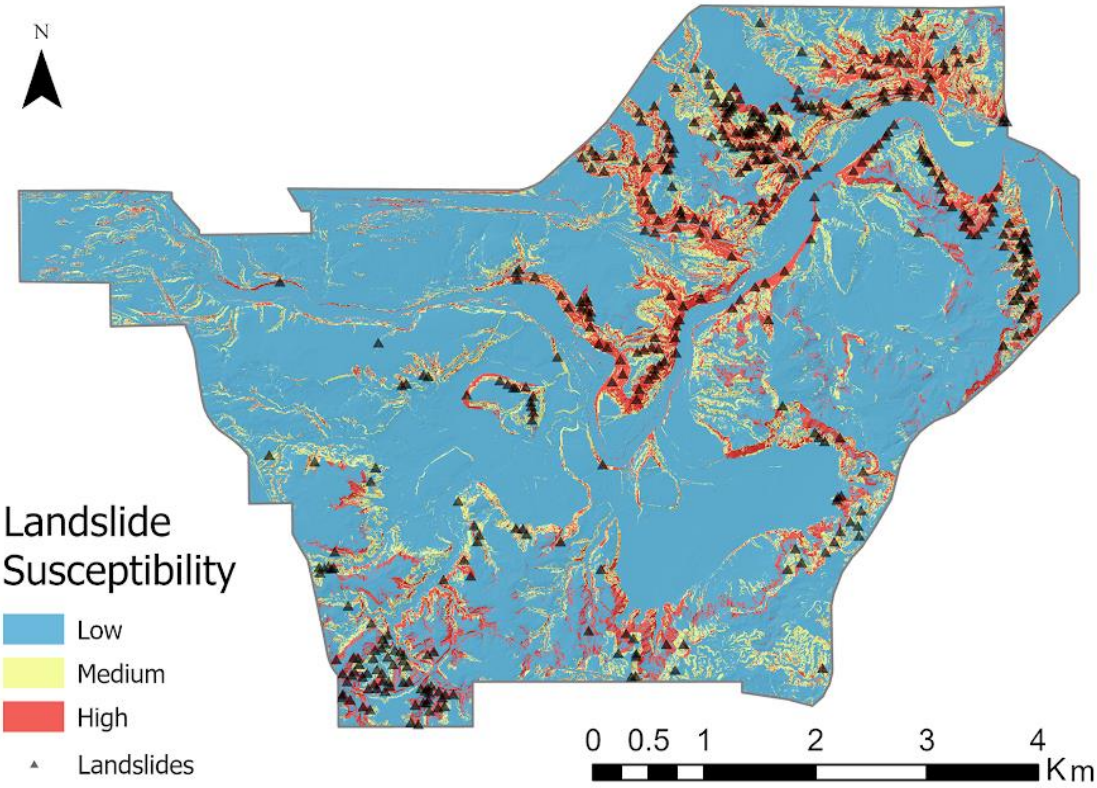

Figure 12. Landslide susceptibility map for Jay Cooke State Park.

with flatter slopes (2.4-4.3 degrees) are likely the result of quasi-complete data separation because none of the slope failures in this dataset occurred on slope angles of 2.4-4.3 degrees.

Table 7. Simple LR model summary results for Lake Superior South watershed:

	Estimate	Std. Error	P-value
(Intercept)	-5.74	0.71	<0.001
Slope (2.6-4.3)	-13.82	429.82	0.97
Slope (4.3-13.1)	3.17	0.73	<0.001
Slope (13.1-23.5)	8.09	0.72	<0.001
Slope (23.5-31.3)	9.95	0.78	<0.001
Slope (31.3-66.3)	10.25	0.80	<0.001

Table 8. Confusion matrix for simple LR model in the Lake Superior South watershed:

Actual	Predicted	
	Non-Slide	**Slide**
Non-Slide	463	25
Slide	21	453
Accuracy	**95.2%**	

The multivariate LR analysis of slope stability in LSSW determined that slope, substrate, k-factor, depth to bedrock, and distance to stream were all relevant variables for predicting landslides. Slope was weighted more heavily than substrate, k-factor, depth to bedrock, and distance to streams. Clay has a strong relationship with slope stability but it should be noted that it also has a high standard error (1336.37) and p-value (0.99). This is likely also the result of quasi-complete data separation because none of the slope failures in this dataset occurred in clay substrates. Similar data separation is causing a high standard error (927.48) and p-value (0.99) for relatively flat slopes (2.6-4.3 degrees). The overall multivariate model predicted landslide occurrence with 95.3% accuracy.

Table 9. Multivariate LR model summary results in Lake Superior South watershed:

	Estimate	Std. Error	P-value
(Intercept)	-5.00	0.92	<0.001
Substrate (Clay)	-20.04	1336.37	0.99
Substrate (Diamicton)	-2.23	0.54	<0.001
Substrate (Gravel)	-1.74	1.21	0.15
Substrate (Sand)	0.79	0.50	0.11
Substrate (Silt)	-2.69	0.92	<0.001
Depth to Bedrock (6-15)	1.10	0.44	0.01
Depth to Bedrock (15-25)	1.65	0.46	<0.001
Depth to Bedrock (25-45)	1.99	0.55	<0.001
Depth to Bedrock (45-66)	1.56	0.52	<0.001
Depth to Bedrock (66-568)	0.82	0.55	0.13
DTS (20-40)	-0.51	0.47	0.28
DTS (40-113)	-0.98	0.50	0.05
DTS (113-260)	-2.82	0.59	<0.001
DTS (260-497)	-2.86	0.56	<0.001
DTS (497-3860)	-1.86	0.60	<0.001
K-factor (0.2-0.23)	-2.11	0.57	<0.001
K-factor (0.23-0.26)	-1.20	0.50	0.02
K-factor (0.26-0.36)	-0.57	0.45	0.21
K-factor (0.36-0.43)	-2.11	0.57	<0.001
K-factor (0.43-0.47)	-3.28	0.73	<0.001
Slope (2.6-4.3)	-14.72	927.48	0.99
Slope (4.3-13.1)	4.20	0.78	<0.001
Slope (13.1-23.5)	9.40	0.84	<0.001
Slope (23.5-31.3)	11.31	0.92	<0.001
Slope (31.3-66.3)	13.02	1.02	<0.001

Table 10. Confusion matrix for multivariate LR model in Lake Superior South watershed:

Actual	Predicted	
	Non-Slide	**Slide**
Non-Slide	464	25
Slide	20	453
Accuracy	**95.3%**	

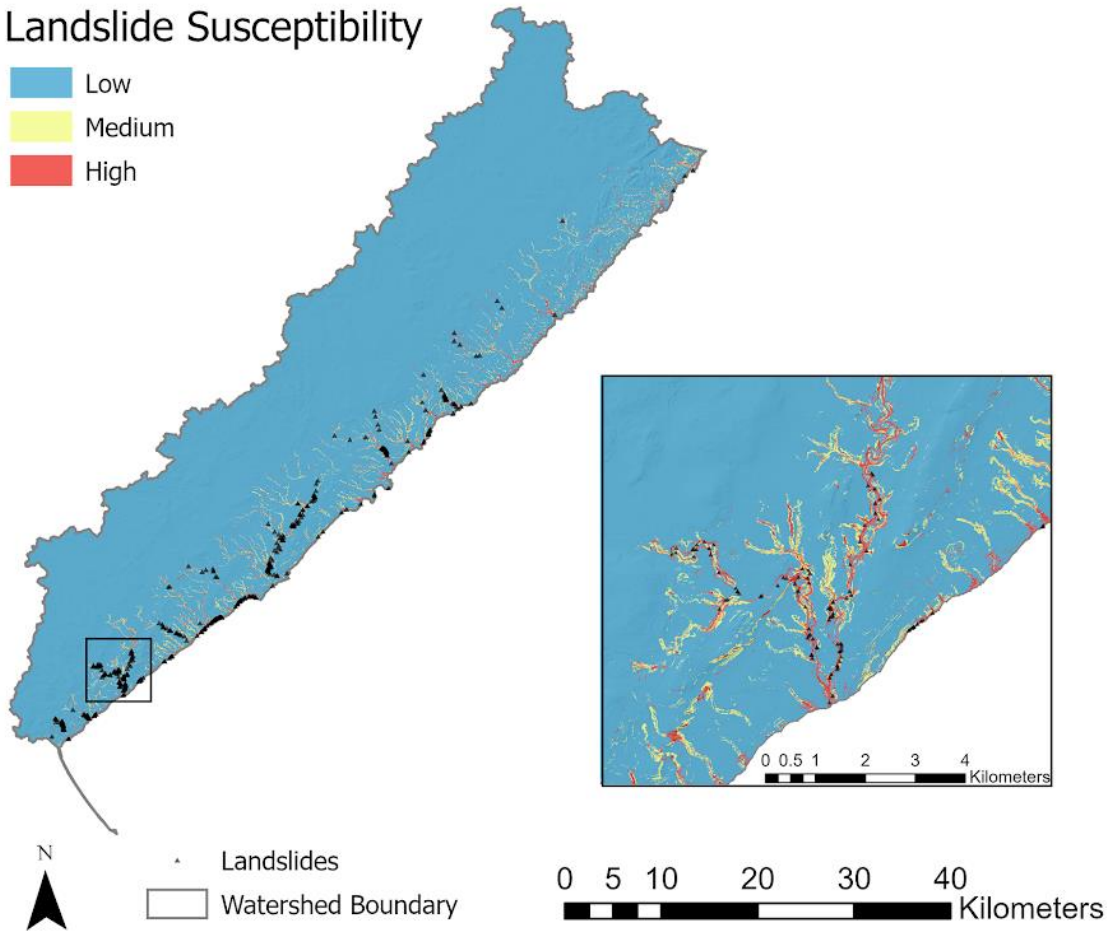

Figure 13. Landslide Susceptibility Map for the Lake Superior South watershed (LSSW).

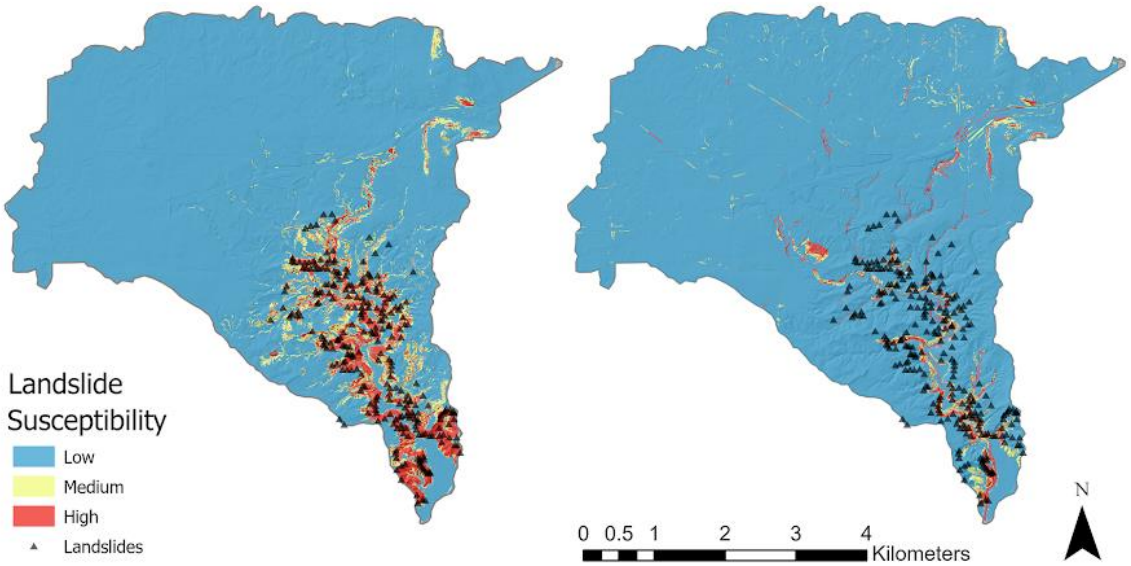

Figure 14. Comparison of the Jay Cooke State Park model (left) and the Lake Superior South watershed model (right) applied to the Mission Creek watershed.

When comparing each model's applicability to the Mission Creek watershed, the Jay Cooke State Park (JCSP) model was more accurate than the Lake Superior South watershed (LSSW) model. The JCSP model predicted landslides with 92% accuracy, while the LSSW model was only 56% accurate at predicting landslide occurrence in this smaller watershed.

Table 11. Confusion matrices for multivariate LR models applied to the Mission Creek watershed. Table on the left shows JCSP model accuracy. Table on the right shows LSSW model accuracy.

Actual	Predicted	
	Non-Slide	**Slide**
Non-Slide	408	41
Slide	26	463
Accuracy	**92%**	

Actual	Predicted	
	Non-Slide	**Slide**
Non-Slide	436	13
Slide	399	90
Accuracy	**56%**	

Discussion

Distribution of Landslides

Landslide distribution across northeastern Minnesota is largely dictated by geomorphic setting. The Red River and Nemadji River basins, located in Carlton county, have a higher density of shallow translational or rotational slope failures than other sub-basins within our study area. These shallow failures occur in glacial lake clays at the interface of sediments and organic soils, often at the average rooting depth (~0.5 meters below the surface). The Jay Cooke State Park and Mission Creek areas cover a mix of ice-marginal, shoreline, and deltaic depositional environments (Breckenridge, 2013). This mixed geomorphic setting produces a combination of failure types with broad ranges in size and age. We observed older deep-seated rotational failures that contain shallower slides and flows along their headscarps or deposits. These sediments are either remobilized through liquefaction as flows or removed by sheet-wash or rilling processes during moderate precipitation events.

The surficial material of the Lake Superior South watershed was deposited in both ice-marginal glacial and paleo-shoreline environments. The majority of slides in these areas are rotational earth slides along outside bends of Lake Superior tributaries or in bluffs along the Lake Superior shoreline. These failures were more concentrated in areas closer to the lake where relief is highest. North St. Louis County was primarily a subglacial setting with drumlin fields and Rogen moraines dispersed across a low gradient area (Kryzer, 2014). These areas appear to only experience slope failure along artificial slopes from road construction or mining activity, suggesting that sub-glacial depositional sediments with low relief are less prone to natural slope failure.

Slope Instability Factors

We found that a multivariate logistic regression (LR) analysis is effective in creating a landslide susceptibility map using slope, distance to streams, depth to bedrock, and substrate. Slope carries most of the predictive power for landslide occurrence, while additional variables only help improve the model accuracy by two to three percent.

Slope angle is the most effective variable for predicting the propensity for landslides regardless of scale, substrate, or geomorphic setting. Studies in mountainous areas also show that slope angle is a significant variable when conducting similar multivariate LR analyses (Chen and Wang, 2007; Mancini et al., 2010; Bai et al., 2010; Yilmaz, 2010; Kavzoglu et al., 2014). In northeastern Minnesota, we also observe that Logistic Regression-based susceptibility models built using only slope work considerably well without including additional variables.

The effectiveness of slope as a dominant predictive variable could be the result of unique circumstances. Using high-resolution lidar data collected in 2011, before the 2012 precipitation event that triggered most of the analyzed slides, created ideal conditions for capturing pre-failure slopes. Most localities do not have access to pre-failure slope data and therefore must measure adjacent slopes or use post-failure data. Because of this, we could be measuring relatively higher slopes. Other studies also found slope to be the most important factor, but it did not have the same independent predictive power as it does in our analysis.

Distance to streams is commonly included in similar LR analyses though it appears to have varied effects reported in the literature. Our results show that distance to streams is a significant variable to consider because down-cutting from channel incision creates areas with steeper gradients and higher relief along main stem river valleys. In a young landscape, like many postglacial landscapes, incision is still actively propagating upstream but has not yet integrated much of the flat upland areas. In our analysis of postglacial landscapes, slope stability increases as the distance to stream increases. This directly opposes what is observed in mountainous areas where high relief and steeper slopes are generally found at the headwaters farther from main stem river channels. A study in the Daunia Mountains of Italy found that increased distances from drainage networks corresponded to more positive regression coefficients that means there is a higher propensity for landslides farther from drainages (Mancini et al., 2010).

Substrate is a consistently relevant geoenvironmental variable for predicting landslide occurrence in many studies. We found that areas mapped as "clay" in the MGS surficial geology map appears to be primarily associated with greater slope stability, which is contrary to the common finding that clays and silty clays correspond to

landslide-prone areas (Mancini et al., 2010; Nandi and Shakoor, 2010). This could be attributed to the broader scale at which the surficial geology was mapped, generalizing "clay" to cover areas with clay-rich tills as well as lacustrine deposits. Alternatively, our results show that landslides are more dominant in areas mapped as diamicton, a substrate that is not included in most studies. We observed that diamicton and lake sediments comprise the majority of slope failures in the Lake Superior watershed. Unfortunately, we cannot discern whether this material's propensity for slope failure is the result of intrinsic characteristics or placement on the landscape. Most of the glacial lake sediments are closer to Lake Superior where sediment packages are thicker and relief is higher. Our analysis revealed that depth to bedrock is a relevant causal factor in our landscape that is not commonly included in other studies. The relationship between material composition and thickness makes their influence difficult to differentiate at such coarse data resolution. However, depth to bedrock had consistently lower p-values than substrate, suggesting greater statistical significance.

Model Performance

Study area and landslide database size can alter the accuracy of multivariate logistic regression analysis, though little experimentation with these factors has occurred in previous research. Since inventory mapping is often a time-consuming and expensive endeavor, state agencies may find themselves wondering how large of an inventory needs to be mapped to perform a useful susceptibility analysis. Can susceptibility modeling in one area be applied to another area where little inventory mapping has been completed? I found that the number of slides, geomorphic setting of the study area, and scale required special consideration for this kind of analysis.

The LR analysis would not function properly with an inventory containing less than 100 landslide polygons and was most effective with several hundred data points for both training and test datasets. Therefore, the size of the study area is only limited by the number of slides concentrated within it. Smaller areas can be used if the landslide density is higher, while larger areas may be required to satisfy the minimum sample size if landslides are sparse.

Most studies have applied logistic regression susceptibility analyses at the thousand to ten thousand square kilometer range (Mancini et al., 2010; Nandi and Shakoor, 2010; Kavzoglu, et al., 2014) with some falling an order of magnitude above (Chen and Wang, 2007) or below (Ayalew et al., 2005). Our analyses in Jay Cooke State Park (35 km^2), Mission Creek watershed (28 km^2), and the Lake Superior South watershed (1616 km^2) examine smaller areas relative to existing studies. Results show that a model run at the thousand km^2 sub-watershed scale or Hydrologic Unit Code 8 (HUC-8) performed with higher accuracy than one at the ten km^2 watershed scale (HUC-12). This could be the result of the resolution of data included in the model. Certain datasets were developed at the county scale and thus did not transfer seamlessly to smaller areas. For example, the depth to bedrock layer was created at the county-scale and therefore reflected a lower resolution at the scale of JCSP. Depth to bedrock became more effective in the LSSW, which is closer to the scale at which the data were created. Many of the datasets used in this analysis were created at the county-wide or statewide scale, which could explain why the LSSW was more accurate than the JCSP model. Because data resolution is a limiting factor, I recommend that this analysis be applied at scales larger than HUC-12 but not much larger than the HUC-8 scale if relying on environmental factors mapped at statewide scales.

Most landslide susceptibility studies have focused on testing several types of susceptibility models over the same area. The research presented here helps address the inverse question: under what conditions can a single susceptibility model developed in one study area be applied to another area? We found that the geomorphic setting has an impact on transferability. The LSSW model did not function effectively when transferred to the Mission creek watershed, which represents a different geomorphic setting. The JCSP model, however, performed well in the adjacent Mission Creek watershed because they share similar geomorphic characteristics. Our study suggests that transferability is better when conducted across similar scales and geomorphic settings.

Climate & Hydrology

Climate change in northeastern Minnesota forecasts an increased risk for high-intensity storms (Blumenfeld, 2016). Erosion from higher stream discharges and stronger

wave velocities will be worsened by increased storminess and will likely trigger more mass-wasting events in the future. Lake Superior water levels also experience natural near-decadal oscillations and 2020 water levels are some of the highest levels on record (Watras et al., 2013; NOAA data viewer). Water levels are also slowly rising near the St. Louis River estuary in response to natural isostatic rebound, compounding the effects from climate change and cyclical lake level adjustments on coastal erosion. There should be an increase in slope failure events while water levels remain elevated. Our landslide inventory reflects which areas are most sensitive to the effects of climate change on fluvial and coastal erosion, allowing us to anticipate how these events may alter the landscape in the future.

Current projections reveal a warmer and wetter climate for the region with an increased possibility for short duration heavy precipitation events (Blumenfeld, 2016). The 500-year flood event that happened in 2012 is a good example of what we are likely to see when these types of events happen more frequently. Repeat lidar data from before and after the 2012 flood reveals that 60% of mapped slope failures were either triggered or re-activated as a result of the June 2012 precipitation event. The flooding had a magnified effect on slope stability because of saturated soil conditions from an already rainy spring, with May 2012 as one of the wettest recorded Mays in Duluth's history (Czuba et al., 2012). This highlights the significance of precipitation and flooding on slope stability in the region. High soil moisture conditions tend to increase run-off discharge to streams and rivers, increasing the stream power that drives toe-cutting erosion along outside bends. Groundwater seepage is also increased by elevated soil moisture conditions, under which water can emerge from bluff faces with enough force to cause mass-wasting from seepage erosion (Dunne, 1990).

Streambank erosion has evolved to the point of mass bluff failure in most Lake Superior tributaries because of ongoing channel incision from knickpoints initiated by paleo-lake level changes. 55% of the inventory is within 30 meters of a stream or river channel which demonstrates the relevance of river incision on slope failure in this region. Relief is highest near streams because of the high level of incision that most streams in the region have experienced since glaciers receded from the landscape. Toe-cutting erosion causes mass wasting only in places where there is enough relief to trigger mass

bluff failure. This process is apparent in the LR analysis of "distance to stream" from the LSSW model which shows increasing stability as you move farther away from channels. There should be an escalation in mass bluff failure along stream corridors as more frequent storms contribute to higher stream discharges.

Coastal erosion along the shoreline of Lake Superior is increasing because of rising water levels and increased frequency of storms. Great Lakes water levels rise and fall in near-decadal oscillations that are largely driven by evaporation (Watras et al., 2013). Monthly-averaged water level data from NOAA monitoring stations reveal that we are on the rising limb of one of these oscillations and have reached new record highs in 2019 (NOAA data viewer). Slope failures along the shoreline comprise 8% of our inventory and include both rotational slumps in till or rockfall zones in bedrock cliffs along the shoreline. Increased storminess also increases wave action which leads to greater toe-cutting and thus exacerbates coastal bluff erosion (Johnson and Johnston, 1995; Mickelson et al., 2020). Another factor in lake level changes is the influence of isostatic rebound. Relative to the outlet of Lake Superior at Point Iroquois, MI, the shoreline at Duluth, MN, is falling at a rate of roughly 2.5 mm per year, while the shoreline at Rossport, Ontario, is rising at a rate of roughly 3.0 mm per year (Mainville and Craymer, 2005). This differential uplift leads to higher water levels towards the western arm of Lake Superior and intensifies the impact of wave action on coastal erosion. Based on what we see in our landslide inventory from past storm events, climate change should increase the frequency of coastal landslides in northeastern Minnesota from increased storminess during times of higher lake levels.

Study Limitations & Future Work

This study establishes a framework for understanding slope failure processes in low gradient landscapes shaped by glaciation. The products from this research will also be useful to Minnesota landowners and emergency managers with goals of minimizing risks to property, infrastructure, and public safety. This research has created a resource that can be used for continued exploration of the physical processes driving slope instability in postglacial landscapes.

It is important to remember that this database represents a snapshot in time. We are creating a landslide inventory circa 2019 that will require ongoing attention as hillslopes continue to evolve. This was a three-year study aimed at compiling past and present slope failures. However, slopes will continue to fail and for this resource to remain relevant and useful to the public and land managers, the mapping and updating effort should be taken over by a state agency or other organization.

There is also a lot more that can be done with this dataset than the work completed by this study. Further analysis should include an assessment of precipitation, a primary driver for slope failure, which was not explored in this analysis. Rainfall is one of the most influential variables in slope stability because of its ability to both increase the shear stress and decrease the shear strength of unconsolidated materials on a slope. Unfortunately, time and resource constraints did not allow us to investigate the magnitude and duration of precipitation necessary to trigger mass-movements in northeastern Minnesota. Using this inventory and climatic data from the 2012 flood and other events, one could generate an event-based model that explores the influence of precipitation and flooding on mass-wasting.

These susceptibility maps were developed using broad spatial data and therefore the areas labeled as high susceptibility would require site-specific monitoring and data. Future work should include detailed monitoring and collection of site-specific information to investigate the rheology of different glacial sediments. Data on soil moisture, hydraulic conductivity, and material shear strength would improve our understanding of local conditions. This research does not replace the need for Geotechnical assessments and any areas mapped as high susceptibility zones by this research require further investigation.

Conclusions

I compiled an inventory of landslides and other mass-movements throughout the Lake Superior Watershed in northeastern Minnesota. I then used this inventory and a combination of publicly available geo-spatial datasets to generate landslide susceptibility assessments. The following conclusions about slope stability in the Lake Superior Watershed in northeastern Minnesota can be drawn based on my analyses:

- Slope, depth to bedrock, distance to streams, and substrate are statistically significant variables for predicting landslides using a multivariate logistic regression analysis.
- Slope, as a singular independent variable, predicts the majority of landslides in these areas.
- Susceptibility models have greater accuracy when implemented at a scale similar to the resolution of the geoenvironmental factors used for the analysis (83% in JCSP; 95% in LSSW).
- Thick, unconsolidated glacial material is more vulnerable to sliding near streams during floods and heavy-precipitation events. This trend is magnified by the fact that most of the relief in these young, incising basins is isolated along stream corridors and most of the uplands are not integrated by developed drainage networks.
- Paleo-geomorphic settings such as continental ice-margins, glacial lake-basins, or paleo-shoreline environments determine the material and structural properties of the substrate in which landslides occur, making them important to consider when assessing landslide susceptibility.

These findings and the methodology used provide a framework for the mapping and assessment of landslide susceptibility in the upper Midwest and other similar postglacial landscapes. The primary limitation to these findings is that they overwhelmingly capture this landscape's response to a particular precipitation event in 2012. Methods developed in this study should be modified to accommodate available data in regions of interest,

therefore I list the following recommendations for future assessment in other parts of Minnesota:

- Landslide detection and inventory mapping are the basis for landslide susceptibility and geo-hazard assessments. The scale of the susceptibility analysis is dictated in part by the density of landslides as the number of landslides is a limiting factor for the size of the study area used in a susceptibility analysis.
- Multivariate logistic regression analysis can provide reliable susceptibility models. To improve predictability, study areas should be chosen that align with geomorphic boundaries and at scales that closely match the resolution of regional datasets.
- Slope, depth to bedrock, distance to streams, and substrate are critical variables to consider when studying landslides in young, previously glaciated areas.

Understanding how these types of areas are geologically and geomorphically unique allows us to better predict how they will adjust to climatic changes. Landslides and other mass-wasting events are abundant in northeastern Minnesota and will likely become more common as the regional climate trends toward warmer and wetter conditions.

References

Aleotti, P. and Chowdhury, R. (1999). Landslide hazard assessment: summary review and new perspectives. *Bulletin of Engineering Geology and the Environment*, *58*(1), 21-44. https://doi.org/10.1007/s100640050066.

Ayalew, L., Yamagishi, H., Marui, H. and Kanno, T. (2005). Landslides in Sado Island of Japan: Part II. GIS-based susceptibility mapping with comparisons of results from two methods and verifications. *Engineering geology*, *81*(4), 432-445. https://doi.org/10.1016/j.enggeo.2005.08.004.

Bai, S.B., Wang, J., Lü, G.N., Zhou, P.G., Hou, S.S. and Xu, S.N. (2010). GIS-based logistic regression for landslide susceptibility mapping of the Zhongxian segment in the Three Gorges area, China. *Geomorphology*, *115*(1-2), 23-31. https://doi.org/10.1016/j.geomorph.2009.09.025.

Belmont, P. (2011). Floodplain width adjustments in response to rapid base level fall and knickpoint migration. *Geomorphology*, *128*(1-2), 92-102. https://doi.org/10.1016/j.geomorph.2010.12.026.

Blumenfeld, K. (2016). *How the Climate of Minnesota is and is not changing*, [PowerPoint slides] Urban Forestry/Climate Change Symposium. http://www.mnstac.org/uploads/2/0/9/3/20933948/blumenfeld.pdf.

Brardinoni, F., Slaymaker, O. and Hassan, M.A. (2003). Landslide inventory in a rugged forested watershed: a comparison between air-photo and field survey data. *Geomorphology*, *54*(3-4), 179-196. https://doi.org/10.1016/S0169-555X(02)00355-0.

Burns, W.J. and Madin, I.P. (2009). Protocol for inventory mapping of landslide deposits from light detection and ranging (LiDAR) imagery. *Oregon Department of Geology and Mineral Industries.* https://www.oregongeology.org/pubs/dds/slido/sp-42_onscreen.pdf.

Carrara, A. and Merenda, L. (1976). Landslide inventory in northern Calabria, southern Italy. *Geological Society of America Bulletin*, *87*(8), 1153-1162. https://doi.org/10.1130/0016-7606(1976)87%3C1153:LIINCS%3E2.0.CO;2.

Castro, J. and Reckendorf, F. (1995). Effects of sediment on the aquatic environment: Potential NRCS Actions to Improve Aquatic Habitat – Working Paper No. 6. *US Department of Agriculture, Natural Resources Conservation Service, Oregon State University, Department of Geosciences.* https://www.nrcs.usda.gov/wps/portal/nrcs/detail/national/technical/?cid=nrcs143_014201.

Chen, Z. and Wang, J. (2007). Landslide hazard mapping using logistic regression model in Mackenzie Valley, Canada. *Natural Hazards*, *42*(1), 75-89. https://doi.org/10.1007/s11069-006-9061-6.

Chiba, T., Kaneta, S., and Suzuki, Y. (2008). Red relief image map: New visualization method for three dimensional data. *Remote Sensing and Spatial Information Science 37*(2).

Crawford, M.M. (2012). Using LiDAR to Map Landslides in Kenton and Campbell Counties, Kentucky. *Kentucky Geological Survey, ser. 12. Report of Investigations 24*. https://kgs.uky.edu/kgsweb/olops/pub/kgs/ri24_12.pdf.

Crozier, M.J. (2010). Deciphering the effect of climate change on landslide activity: A review. *Geomorphology*, *124*(3-4), 260-267. https://doi.org/10.1016/j.geomorph.2010.04.009.

Cruden, D.M. and Varnes, D.J. (1996). Landslide Types and Processes. In R.L. Schuster & A.K. Turner (Eds.), *Landslides: Investigation and Mitigation* (Ch. 3, pp. 36-75). Washington: National Academy Press.

Czuba, C.R., Fallon, J.D. and Kessler, E.W. (2012). Floods of June 2012 in northeastern Minnesota. *U.S. Geological Survey Scientific Investigations Report 2012–5283*. https://pubs.usgs.gov/sir/2012/5283/sir2012-5283.pdf.

Day, S. S., Gran, K. B., Belmont, P., & Wawrzyniec, T. (2013). Measuring bluff erosion part 1: Terrestrial laser scanning methods for change detection. *Earth Surface Processes and Landforms*, *38*(10), 1055-1067. https://doi.org/10.1002/esp.3353.

DeLong, S.B., Engle, Z.T., Hammer, M., Richard, E.M., Gran, K.B., Breckenridge, A.J., Jalobeanu, A. (2020). Revisiting the 2012 Duluth, MN Extreme Precipitation Event: Characterizing the Extent and Magnitude of Landslides, Erosion, and Sedimentation Using Repeat Lidar and Object-Based Image Analysis. *Geological Society of America Abstracts with Programs*. Vol. 52, No. 5, ISSN 0016-7592 doi: 10.1130/abs/2020NC-348208

Dunne, T. (1990). Chapter 1. Hydrology Mechanics, and Geomorphic Implications of Erosion by Subsurface Flow. In *Geological Society of America Special Paper 252, Geological Society of America.* https://doi.org/10.1130/SPE252-p1.

Engle, Z.T., DeLong, S.B., Bartley, J.K., Blumentritt, D., Breckenridge, A.J., Day, S.S., Gran, K.B., Jennings, C.E., Larson, P.H., Mcdermott, J.A., Triplett, L.D., Wickert, A.D. (2020). Towards Design of a Landslide Inventory Geodatabase for Minnesota. *Geological Society of America Abstracts with Programs*. Vol. 52, No. 5, ISSN 0016-7592, doi: 10.1130/Abs/2020nc-348185

Fabbri, A.G., Chung, C.J.F., Cendrero, A. and Remondo, J. (2003). Is prediction of future landslides possible with a GIS? *Natural Hazards*, *30*(3), 487-503. https://doi.org/10.1023/B:NHAZ.0000007282.62071.75.

Finley-Blasi, L. (2006). Detrital Zircon Age Analysis of the Fond Du Lac and Hinckley Sandstone Formations of Northern Minnesota. In *19th Annual Keck Symposium, Cam Davidson, Amherst, Mass*. https://keckgeology.org/files/pdf/symvol/19th/minnesota/finley-blasi.pdf.

Fitzpatrick, F.A., Ellison, C.A., Czuba, C.R., Young, B.M., and McCool, M.M. (2016). Geomorphic responses of Duluth area streams to the June 2012 flood, Minnesota. *U.S. Geological Survey Scientific Investigations Report 2016–5104*. http://dx.doi.org/10.3133/sir20165104.

Gran, K. (2017). Landslide hazards and impacts on Minnesota's natural environment. *Environment and Natural Resources Trust Fund (ENRTF) M.L. 2017 LCCMR Work Plan*, Chp. 96, Sec. 2, Subd. 03i.

Guzzetti, F., Cardinali, M., Reichenbach, P. and Carrara, A. (2000). Comparing landslide maps: A case study in the upper Tiber River Basin, central Italy. *Environmental Management 25*(3), 247-263. https://doi.org/10.1007/s002679910020.

Guzzetti, F., Carrara, A., Cardinali, M. and Reichenbach, P. (1999). Landslide hazard evaluation: a review of current techniques and their application in a multi-scale

study, Central Italy. *Geomorphology 31*(1-4), 181-216. https://doi.org/10.1016/S0169-555X(99)00078-1.

Guzzetti, F., Mondini, A.C., Cardinali, M., Fiorucci, F., Santangelo, M. and Chang, K.T. (2012). Landslide inventory maps: New tools for an old problem. *Earth-Science Reviews*, *112*(1-2), 42-66. https://doi.org/10.1016/j.earscirev.2012.02.001.

Guzzetti, F., Reichenbach, P., Ardizzone, F., Cardinali, M. and Galli, M. (2006). Estimating the Quality of Landslide Susceptibility Models. *Geomorphology*, *81* (1-2), 166-184. https://doi.org/10.1016/j.geomorph.2006.04.007.

Hall, Leah. (2016). *Monitoring Bluff Erosion Rates Using Terrestrial Laser Scanning on Minnesota's North Shore Streams.* Master's thesis, University of Minnesota Digital Conservancy. http://hdl.handle.net/11299/181794.

Hagerty, D. J. (1991). Piping/sapping erosion. I: Basic considerations. *Journal of Hydraulic Engineering* 117(8), 991-1008.

Handler, S., Duveneck, M.J., Iverson, L., Peters, E., Scheller, R.M., Wythers, K.R., Brandt, L., Butler, P., Janowiak, M., Shannon, P.D. and Swanston, C. (2014). Minnesota forest ecosystem vulnerability assessment and synthesis: A report from the Northwoods Climate Change Response Framework project. *Gen. Tech. Rep. NRS-133. Newtown Square, PA; US Department of Agriculture, Forest Service, Northern Research Station*, 1-228. https://doi.org/10.2737/NRS-GTR-133.

Highland, L. and Bobrowsky, P. (2008). The Landslide Handbook — A Guide to Understanding Landslides, *US Geological Survey Circular 1325*. https://pubs.usgs.gov/circ/1325/pdf/C1325_508.pdf.

Hobbs, H.C. (2003). M-137 Surficial geology of the Knife River quadrangle, St. Louis and Lake Counties, Minnesota. *Minnesota Geological Survey. Retrieved from the University of Minnesota Digital Conservancy*, http://hdl.handle.net/11299/514.

Hobbs, H.C. (2004). Late Wisconsin Superior-Lobe deposits in the Superior Basin northeast of Duluth. In Severson, M.J. and Heinz, J. (Eds.), *Proceedings of the Institute on Lake Superior Geology, 50th Annual Meeting, Field Trip Guidebook 50*, 86–98.

Hobbs, H.C., Breckenridge, A., Miller, J.D., Hudak, G.J., Wittkop, C. and McLaughlin, P.I. (2011). Ice advances and retreats, inlets and outlets, sediments and strandlines of the western Lake Superior basin. *Archean to Anthropocene: Field Guides to the Geology of the Mid-continent of North America, GSA Field Guide 24*, 299-315.

Hooke, J. M. (1979). An analysis of the processes of river bank erosion. *Journal of Hydrology 42*, 39-62. https://doi.org/10.1016/0022-1694(79)90005-2

Hungr, O., Leroueil, S. and Picarelli, L. (2014). The Varnes classification of landslide types, an update. *Landslides 11*(2), 167-194. https://doi.org/10.1007/s10346-013-0436-y.

Intergovernmental Panel on Climate Change [IPCC] (2007). Climate change 2007: synthesis report. Contribution of Working Groups I, II, and III to the Fourth Assessment Report of the Intergovernmental Panel on Climate Change. [Core Writing Team, Pachauri, R.K. and Reisinger, A., eds.]. *Geneva, Switzerland: Intergovernmental Panel on Climate Change*. https://archive.ipcc.ch/publications_and_data/ar4/syr/en/main.html.

Jaboyedoff, M., Oppikofer, T., Abellán, A., Derron, M., Loye, A., Metzger, R., and Pedrazzini, A. (2012). Use of LIDAR in landslide investigations: a review. *Natural Hazards 61*, 5–28. https://doi.org/10.1007/s11069-010-9634-2.

Jasperson, J., Beaster, T., Jasperson, J., and Thompson, A. (2018). Lake Superior North Stressor Identification Report, *Minnesota Pollution Control Agency*. https://www.pca.state.mn.us/sites/default/files/wq-ws5-04010101a.pdf.

Jennings, C.E., Presnail, M., Kurak, E., Meier, R., Schmidt, C., Palazzolo, J., Jiwani, S., Waage, E. and Feinberg, J.M. (2016). Historical Landslide Inventory for the Twin Cities Metropolitan Area. *Minnesota Department of Natural Resources: Division of Ecological and Water Resources*. https://files.dnr.state.mn.us/waters/watermgmt_section/shoreland/landslide-inventory.pdf.

Johnson, B. L. and Johnston, C. A. (1995). Relationship of Lithology and Geomorphology to Erosion of the Western Lake Superior Coast, *Journal of Great Lakes Research 21(1)*, 3–16. https://doi.org/10.1016/S0380-1330(95)71016-4.

Kavzoglu, T., Sahin, E.K. and Colkesen, I. (2014). Landslide susceptibility mapping using GIS-based multi-criteria decision analysis, support vector machines, and logistic regression. *Landslides 11*(3), 425-439. https://doi.org/10.1007/s10346-013-0391-7.

Kling, G.W., K. Hayhoe, L.B. Johnson, J.J. Magnuson, S. Polasky, S.K. Robinson, B.J. Shuter, M.M. Wander, D.J. Wuebbles, D.R. Zak, R.L. Lindroth, S.C. Moser, and M.L. Wilson (2003). Confronting Climate Change in the Great Lakes Region: Impacts on our Communities and Ecosystems. Union of Concerned Scientists, Cambridge, Massachusetts, and Ecological Society of America, Washington, D.C. Available at https://www.ucsusa.org/sites/default/files/2019-09/greatlakes_final.pdf

Kryzer, R. (2014). Rögen Moraine as a Transitional Bedform in an Erosional Subglacial System. *Duluth Journal of Undergraduate Research, University of Minnesota Digital Conservancy*. http://hdl.handle.net/11299/187026.

Lahti, L., Hansen, B., Nieber, J., and Magner, J. (2013). Lake Superior Streams Sediment Assessment: Phase I. *University of Minnesota, Department of Bioproducts and Biosystems Engineering, St. Paul, MN*. https://www.pca.state.mn.us/sites/default/files/wq-b2-04.pdf.

Lee, S. and Sambath, T. (2006). Landslide susceptibility mapping in the Damrei Romel area, Cambodia using frequency ratio and logistic regression models. *Environmental Geology 50*(6), 847-855. https://doi.org/10.1007/s00254-006-0256-7.

Lee, D.H. and Southam, C.F. (1994). Effect and Implications of Differential Isostatic Rebound on Lake Superior's Regulation Limits. *Journal of Great Lakes Research 20(2)*, 407-415. https://www.glerl.noaa.gov/pubs/fulltext/1994/19940005.pdf

Leverett, F. (1929). Moraines and Shore Lines of the Lake Superior Basin. *U.S. Geological Survey, Professional Paper 154-A.* Washington: United States Government Printing Office.

Lusardi, B.A. and Dengler, E.L. (2017). Minnesota at a Glance: Quaternary Glacial Geology. *Minnesota Geological Survey, University of Minnesota Digital Conservancy*. http://hdl.handle.net/11299/59427.

Mainville, A., Craymer, M.R. (2005). Present-day tilting of the Great Lakes region based on water level gauges. *Geological Society of America Bulletin 117*(7-8), 1070–1080. https://doi.org/10.1130/B25392.1

Mancini, F., Ceppi, C., and Ritrovato, G. (2010) GIS and statistical analysis for landslide susceptibility mapping in the Daunia area, Italy. *Nat. Hazards Earth Syst. Sci. 10*, 1851–1864. https://doi.org/10.5194/nhess-10-1851-2010.

Manopkawee, P. (2015). *Identifying Erosional Hotspots in Duluth-Area Streams after the 2012 Flood Using High-Resolution Aerial Lidar Data*. Master's thesis, University of Minnesota Digital Conservancy. http://hdl.handle.net/11299/174810.

Martha, T.R., Kerle, N., Jetten, V., Van Westen, C.J., Kumar K.V. (2010). Characterising spectral, spatial and morphometric properties of landslides for semi-automatic detection using object-oriented methods, *Geomorphology, Elsevier B.V.* 116(1–2), 24–36. https://doi.org/10.1016/j.geomorph.2009.10.004.

Mickelson, D., Stone, J., Hochschild, J. (2020). Continuing high lake levels are leading to severe erosion of western Lake Superior's clay bluffs in Wisconsin. *Geological Society of America Abstracts with Programs. Vol. 52, No. 5, ISSN 0016-7592*, doi: 10.1130/Abs/2020nc-348004

Nandi, A. and Shakoor, A. (2010). A GIS-based landslide susceptibility evaluation using bivariate and multivariate statistical analyses. *Engineering Geology 110*(1-2), 11-20. https://doi.org/10.1016/j.enggeo.2009.10.001.

Natural Resource Conservation Service (1998). Erosion and Sedimentation in the Nemadji River Basin: Nemadji River Basin Project Final Report. *USDA Natural Resources Conservation Service (NRCS), U.S. Forest Service*. https://dnr.wi.gov/topic/greatlakes/documents/NemadjiRiverBasinProjectReport.pdf.

Neitzel, G.D. (2014). *Monitoring event-scale stream bluff erosion with repeat terrestrial laser scanning: Amity Creek, Duluth, MN*. Master's thesis, University of Minnesota Digital Conservancy. http://hdl.handle.net/11299/163326.

Nieber J.L., Wilson, B.N., Ulrich, J.S., Hansen, B.J., Canelon, D.J. (2008). Assessment of Streambank and Bluff Erosion in the Knife River Watershed. *Department of Bioproducts and Biosystems Engineering, University of Minnesota, St. Paul, Minnesota.*

Ojakangas, R. and Matsch, C. (1982). *Minnesota's Geology*. University of Minnesota Press.

Ozdemir, A. and Altural, T. (2013). A comparative study of frequency ratio, weights of evidence and logistic regression methods for landslide susceptibility mapping: Sultan Mountains, SW Turkey. *Journal of Asian Earth Sciences 64*, 180-197. https://doi.org/10.1016/j.jseaes.2012.12.014

Raupach, M. R., Marland, G., Ciais, P., Le Quéré, C., Canadell, J. G., Klepper, G., & Field, C. B. (2007). Global and regional drivers of accelerating CO2 emissions. *Proceedings of the National Academy of Sciences*, *104*(24), 10288-10293. https://doi.org/10.1073/pnas.0700609104

R Core Team (2019). R: A language and environment for statistical computing. R Foundation for Statistical Computing, Vienna, Austria. https://www.r-project.org/

Reichenbach, P., Rossi, M., Malamud, B.D., Mihir, M. and Guzzetti, F. (2018). A review of statistically-based landslide susceptibility models. *Earth-Science Reviews 180*, 60-91. https://doi.org/10.1016/j.earscirev.2018.03.001

Ritter, D., Kochel, R., and Miller, J. (2002). *Process Geomorphology* (4th ed.) New York, NY: McGraw-Hill. 95-133.

Sandberg, J., Anderson, J., Lundeen, B., Sather, N., Bourdaghs, M., Vaughan, S., Nerem, K., Jasperson, J., Christopherson, D., Monson, B., Nelson, S., Parson, K., Grayson, S. (2017). Lake Superior – North Watershed Monitoring and Assessment Report. *Minnesota Pollution Control Agency, St. Paul, MN*. https://www.pca.state.mn.us/sites/default/files/wq-ws3-04010101b.pdf

Saunders, S., Findlay, D., Easley, T., and Spencer, T. (2012). Doubled Trouble: More Midwestern Extreme Storms. *The Rocky Mountain Climate Organization and the Natural Resources Defense Council.* http://rockymountainclimate.org/images/Doubled%20Trouble.pdf

Schuster, R.L. and Fleming, R.W. (1986). Economic losses and fatalities due to landslides. *Bulletin of the Association of Engineering Geologists 23*(1), 11-28.

Sekely, A.C., Mulla, D.J. and Bauer, D.W. (2002). Streambank slumping and its contribution to the phosphorus and suspended sediment loads of the Blue Earth River, Minnesota. *Journal of Soil and Water Conservation 57*(5), 243-250.

Kraker, D. (2017, October). *5 years after flood, lone road through Jay Cooke state park reopens*. Retrieved from https://www.mprnews.org/story/2017/10/04/jay-cooke-state-park-bridge-reopens-after-flood

Sims, P.K. and Morey, G.B. (1972). Geology of Minnesota: A Centennial Volume. *Minnesota Geological Survey, University of Minnesota Digital Conservancy*, http://hdl.handle.net/11299/59791.

Sinha, T., Cherkauer, K.A., and Mishra, V. (2010). Impacts of Historic Climate Variability on Seasonal Soil Frost in the Midwestern United States. *Journal of Hydrometeorology 11(2),* 229-252. https://doi.org/10.1175/2009JHM1141.1.

Slaughter, S.L., Burns, W.J., Mickelson, K.A., Jacobacci, K.E., Biel, A. and Contreras, T.A. (2017). Protocol for landslide inventory mapping from lidar data in Washington State. *Washington Geological Survey Bulletin 82*, 27p. http://www.dnr.wa.gov/Publications/ger_b82_landslide_inventory_mapping_protocol.zip

Spiker, E.C., and Gori, P.L. (2000). National landslide hazards mitigation strategy: a framework for loss reduction. *US Dept. of the Interior, US Geological Survey Open-File Report 00-450*. https://pubs.usgs.gov/of/2000/ofr-00-0450/ofr-00-0450.pdf.

Venables, W.N. and Ripley, B.D. (2002). *Modern Applied Statistics with S*. (4th ed.) Springer, New York. ISBN 0-387-95457-0

Wick, M.J. (2013). *Identifying Erosional Hotspots in Streams along the North Shore of Lake Superior, Minnesota using High-Resolution Elevation and Soils Data*. Master's thesis, University of Minnesota Digital Conservancy, http://hdl.handle.net/11299/189260.

Watras, C.J., Read, J.S., Holman, K.D., Liu, Z., Song, Y.Y., Watras, A.J., Morgan, S. and Stanley, E.H. (2014). Decadal oscillation of lakes and aquifers in the upper Great Lakes region of North America: Hydroclimatic implications. *Geophysical Research Letters 41*(2), 456-462. https://doi.org/10.1002/2013GL058679.

Wuebbles, D., Cardinale, B., Cherkauer, K., Davidson-Arnott, R., Hellmann, J.J., Infante, D., Johnson, L., de Loe, R., Lofgren, B., Packman, A., and Selenieks, F. (2019).

An Assessment of the Impacts of Climate Change on the Great Lakes. *The Environmental Law & Policy Center: Chicago, IL, USA*. https://elpc.org/wp-content/uploads/2020/04/2019-ELPCPublication-Great-Lakes-Climate-Change-Report.pdf.

Yilmaz, I. (2010). Comparison of landslide susceptibility mapping methodologies for Koyulhisar, Turkey: conditional probability, logistic regression, artificial neural networks, and support vector machine. *Environmental Earth Sciences 61*(4), 821-836. https://doi.org/10.1007/s12665-009-0394-9.

Yokoyama, R., Shirasawa, M., & Pike, R. J. (2002). Visualizing topography by openness: a new application of image processing to digital elevation models. *Photogrammetric engineering and remote sensing*, *68*(3), 257-266.

Appendices

Appendix 1: Historical Landslide Inventory

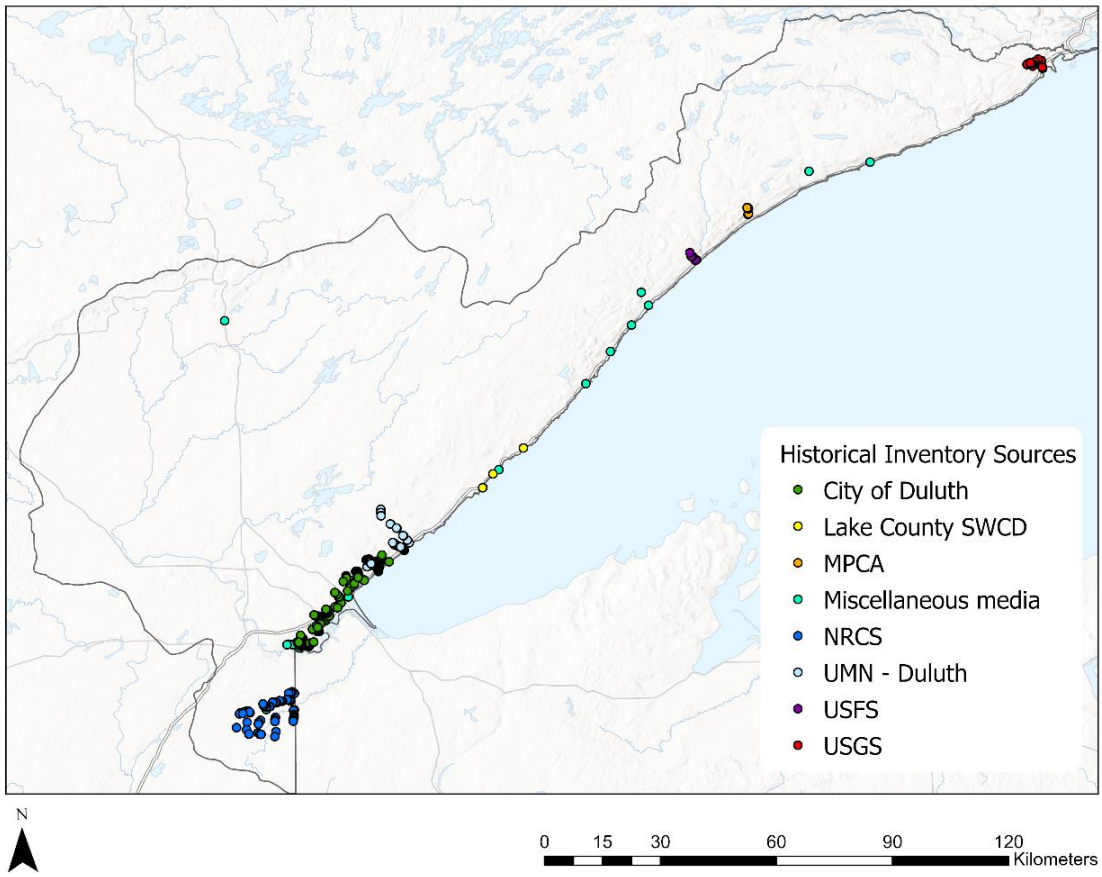

Figure 15: Locations of historically documented landslides within project study area.

Table 12: Attributes for historic inventory points feature class in landslide geodatabase.

Field Name	Description
SLIDE_UNIQUE_ID	A unique landslide identification number assigned to all feature classes and tables related to a landslide. ID's are composed using the quadrangle grid ID (from the 'NG10K4' field of USNG_GRID_10K_MN) followed by an underscore and a 4-digit number beginning with "_0001" that increases consecutively.
DATA_SOURCE	Original source that documented the slide feature (i.e. individual, agency, or institution)
LOCATION_METHOD	Additional information from source dataset which includes exact location method if known (i.e. field data, personal communication, watershed study, etc.)
NAME_SLIDE	Name or number assigned to feature by the original data source.
DATE_SLIDE	Year of slide event (if recorded) or year of source data collection.
CONFIDENCE	1 (potential), 2 (Google Earth verified), 3 (Field verified)
COMMENT	Notes or information from source dataset

Appendix 2: Landslide Inventory and Geodatabase

The geodatabase for the landslide inventory will be available as part of a USGS data release tentatively set for 2021. The data can be found through the USGS data portal once reviewed and made available to the public.

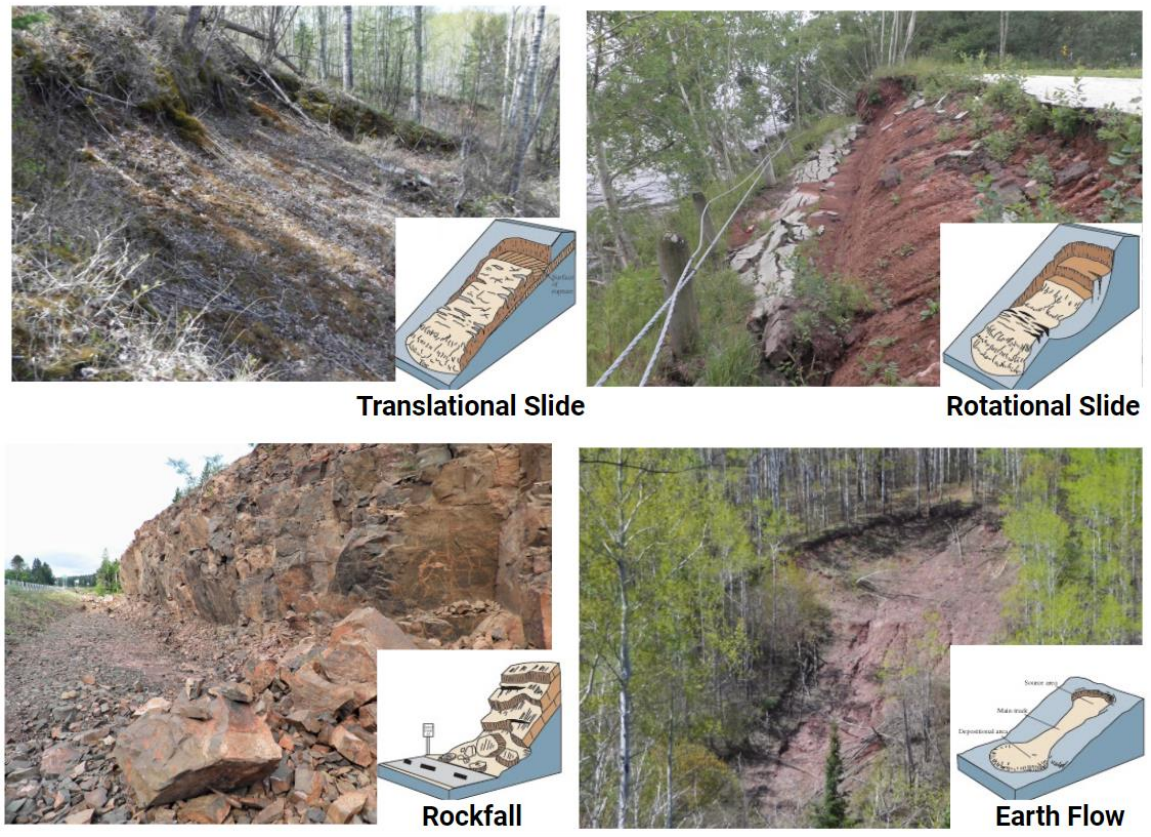

Figure 16: Field photos of four common slide types observed in northeastern Minnesota.

Table 13: Slide Properties table for polygons in landslide geodatabase.

Field Name	Description
SLIDE_UNIQUE_ID	Quadrangle ID followed by a number (ex. MN58_0001, MN58_0002, MN58_000…). Head scarps, deposits, and photo-points for an individual slide will correspond with the same UNIQUE_ID in the "Slide Properties" table.
LOCATION_METHOD	How landslide was located. (i.e. lidar dems, satellite imagery, field work, historical inventory, etc.)
NAME_SLIDE	Nearby stream/road name & ID number (ex. Amity ID_0001)
AGE_EST	(Historic <150yrs) or (Pre-historic >150yrs), estimated based tree growth and vegetation on deposit.
CLASS_SLIDE	Slide type if discernable
GEOLOGIC_MATERIAL	Minnesota Geological Survey D-1 Surficial Geology Map

GEOLOGIC_UNIT	Minnesota Geological Survey D-1 Surficial Geology Map
DEEP_SHALLOW_SEATED	Based on headscarp: < 4ft = Shallow, > 4ft = Deep
LENGTH	NA
WIDTH	NA
DEPTH	NA
SLOPE	Zonal statistics as a table to average slope raster values over entire headscarp polygon
AREA	Shape area
VOLUME	NA
ASPECT	Zonal statistics as a table to average apect raster over the entire headscarp polygon
MVMT_DIRECTION	Azimuth direction of deposit movement from headscarp
CONFIDENCE_CLASS_SLIDE	Sum of points determined by the following: Head scarp = 10 points Flanks = 10 points Deposit = 10 points
CONFIDENCE_LOCATION	GPS photo points = High LiDAR interpretation = Moderate Inferred location = Low
COMMENTS	Any additional notes about slide or how polygon was mapped.

Appendix 3: Detailed Methods for Landslide Susceptibility Mapping

Here are detailed methods for creating a landslide susceptibility map using a multivariate logistic regression approach with ArcGIS Pro, Microsoft Excel, and R statistical programming software.

Study Area Selection and Data Used

This analysis requires an inventory of at least 100 landslide polygons to perform. Many operations require a "mask" within which we generate various raster derivatives, so it is crucial to select a reasonably sized (10 - 1,000 square kilometers) watershed or county boundary based on your computer processing power and inventory size. I will be using Jay Cooke State Park (35 km^2, 419 polygons) as an example.

Table 14: Data used for multivariate logistic regression analysis.

Data	**Source**	**Link**
DEM - Slope and Aspect	MnTOPO	http://arcgis.dnr.state.mn.us/maps/mntopo/
Depth to Bedrock (Carlton County)	MGS - found under subfolder 'grids' - 'dtgd' raster layer - raster calculate from feet to meters	https://conservancy.umn.edu/handle/11299/58760
Land Cover (2011)	NLCD	https://gisdata.mn.gov/dataset/biota-landcover-nlcd-mn-2011
Streams and Rivers	MN DNR - download the geodatabase for the polyline	https://gisdata.mn.gov/dataset/water-strahler-stream-order
Substrate / Lithology	MGS - download options - choose shapefile	https://mngs-umn.opendata.arcgis.com/datasets/surficial-geology-1
Soil K-factor	NRCS SSURGO - download necessary map packages then copy layers to your Arc Project	https://www.arcgis.com/apps/View/index.html?appid=cdc49bd63ea54dd2977f3f2853e07fff
Landslide Polygons	Landslide inventory was created as part of this thesis research.	Shapefiles are pending USGS data release set for 2021.

Phase 1 - Data Compilation and Preparation

Compile basemap rasters:

1. **Substrate** - Polygon to raster with "Lithology" attribute from the MGS surficial geology map. Adjust cell size for WGS coordinates to 0.0001.
2. **Landcover** - sourced from NLCD, extract by mask and resample cell size. Simplify the classes from 15 to 8 different classes by grouping together the following:
    a. The 4 'developed' classifications into a single Developed classification.
    b. The 3 'forest' types into a single Forest classification.
    c. The 'pasture / hay' and 'cultivated crops' into a Cultivated classification
    d. The 2 'wetlands' to a Wetland classification
3. **Aspect** - run the aspect tool using the DEM.
4. **Slope** - generate slope raster from the DEM (*Optional: smooth the slope raster using focal statistics, averaging slopes over a moving circular window with a radius of 3)
5. **Relief** - Focal statistics with the range over a 100x100 moving window. (*Optional: can skip/omit this layer since it is very similar to slope)
6. **Depth to bedrock** - Mosaic to new raster to merge multiple dtb rasters if necessary since these layers are downloaded on a county basis. Be sure to use a raster calculator to convert units in feet (as is on MGS layers) to meters. It can be used as-is from the county atlas, but the resolution leads to a pixelated appearance in the final map product. Since the depth to bedrock layer from the MGS was interpolated from well-log data originally, further interpolation should not significantly impact the data accuracy. Generate a fishnet for the study area with a width of 50 and a length of 50. This should generate a matrix of points that roughly land in each pixel of the depth to bedrock layer. Clip the point file to the study area and use extract multi-point to values to grab a raster value at each point. Use the Natural Neighbor interpolation method to generate the new depth to bedrock raster with a 1x1 cell size.
7. **Distance to streams** - run euclidean distance tool from streams shapefile with 1x1 cell size for output to make a distance to closest stream raster. Set coordinates and extent of study area to process in the environments tab.
8. **Soil erodibility** - Use polygon to raster with the attribute "K-Factor Rock Free" (might also be called "kffact") to rasterize k factor data. Since this data is downloaded by watershed, an additional step may be required to merge multiple rasters depending on the chosen study area.

Prepare dependent variable data table from point fishnets:

1. Import landslide inventory polygons into the ArcGIS workspace (make a copy / new headscarp polygon class/shapefile to work with). We only use the headscarp polygon feature class for this analysis because we want to understand the conditions associated with the failure surface. If you decide, based on your inventory mapping, that the deposit feature class best captures the failure surface conditions, then you may want to include them in your analysis.

2. Create a study area extent polygon that encompasses the headscarp unstable points. The extent may need to be modified depending on how the point generation goes during the following steps. There are multiple ways to go about this: (1) Manually make a shapefile and draw the study area (usually easier if familiar with the study area and unstable polygons distribution). (2) Generate an extent polygon across your headscarp data with minimum bounding geometry (rectangle by area or convex hull, group option “All”), and the ‘Clip’ tool can be used to shrink that extent to your limiting basemap area. (3) Use the Raster domain tool to create a polygon extent of your limiting raster (in this case, clip the polygon down to the extent of the Carlton County Depth to Bedrock layer).

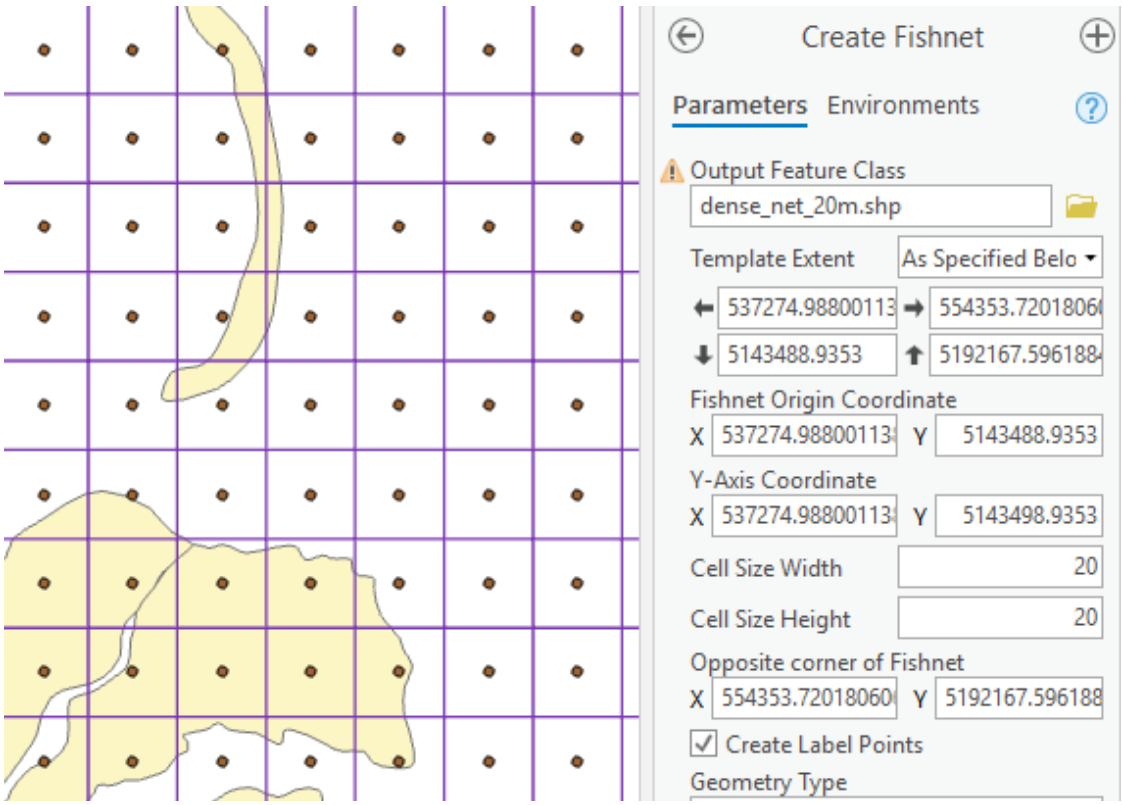

Figure 17: Parameters for creating a dense fishnet of landslide points in ArcGIS Pro.

3. Create fishnets for the study area extent, aiming to get a balanced number of “unstable” (landslide) points and “stable” (non-landslide) points. Start with the unstable points by creating a dense fishnet, setting the study area boundary as the template extent [Figure 17].

4. Retain the dense fishnet points that intersect with a headscarp polygon - Select by location - points intersecting with headscarp polygons. Then export selected data to a new shapefile - right-click fishnet points - data - export features.

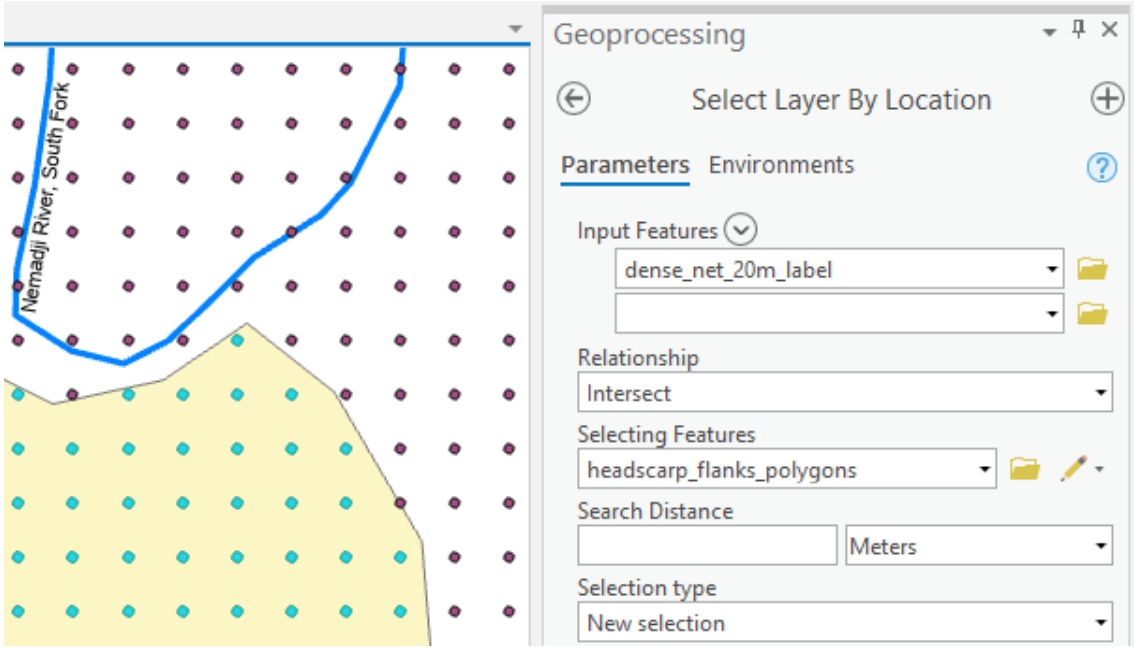

Figure 18: Screen capture showing how to select "unstable" points from fishnet.

5. Create a fishnet of stable points using a much larger cell size for sparse coverage over the full study area. The next step will eliminate some of the points, so it is best to have more stable points as they are easier than the unstable points to remove.

6. Select by location and delete any stable points that intersect with an unstable landslide headscarp polygon. *Optional: run select by location with stream polyline data to delete stable fishnet points within 1-10m of a stream or river.

7. Use the “extract multi values to points” tool for the sparse net points and the dense net points to grab raster pixel values of your geoenvironmental layers at each of the points to build the attribute table. Be mindful to keep the names and order of the variables consistent for both stable and unstable point files.

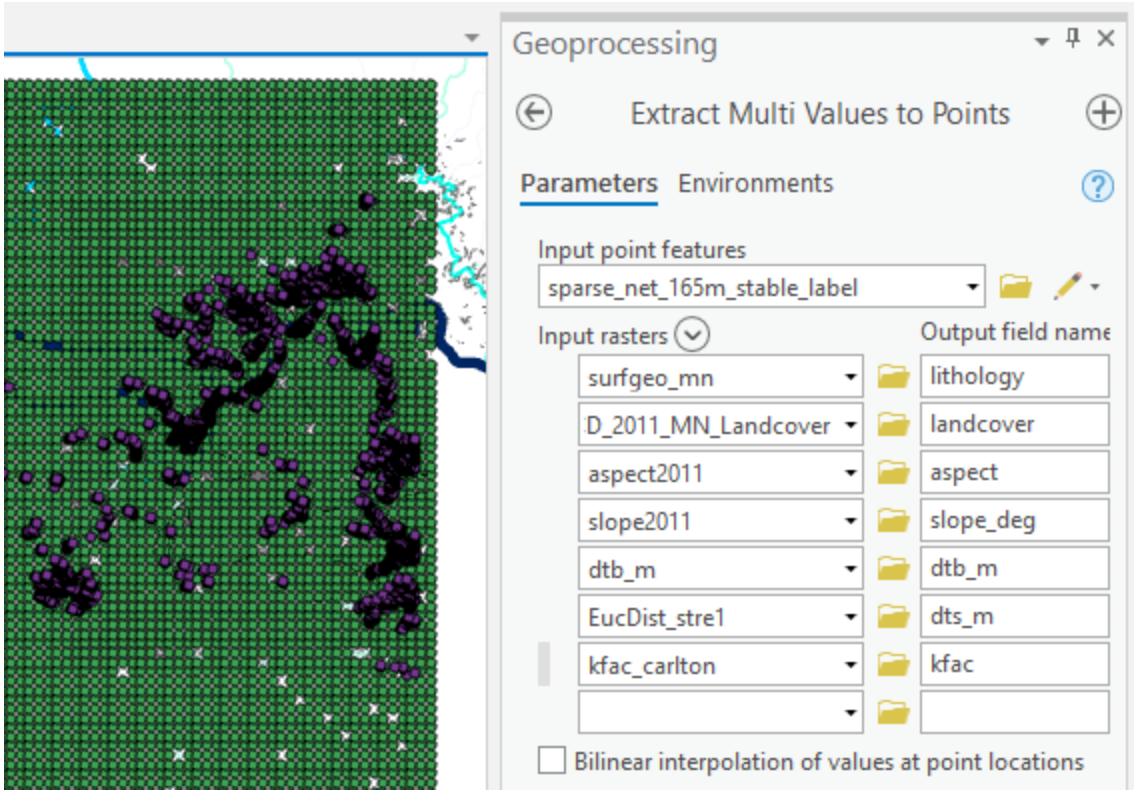

Figure 19: Screen capture showing step 7 of the methodology.

8. Sort your dense and sparse net attribute tables and eliminate any null or incorrect values in either. Use select by attributes to find the -9999 or null values and delete them or manually sort for -9999 or null values in your table and use shift select to delete those points. Can delete points that have a 0 value for distance to stream (dts_m).

9. If the number of stable points and unstable points is highly imbalanced because of the chosen fishnet sizes and scale, the previous four steps may need to be redone until a rough balance is achieved. It is easier to get the dense number set and finalized then start over with making a new sparse net (lower spacing if not enough sparse points compared to dense points, higher spacing if too many sparse points compared to dense points).
    a. *In the Jay Cooke Study Area, we ended up with 1073 unstable (dense - 25m x 25m fishnet) points and 1133 stable (sparse - 175m x 175m) points.*

10. Lastly, run “Add XY coordinates” to calculate the XY coordinates for the sparse and the dense points.

11. Export the attribute tables for your stable and unstable points from Arc to Excel for data clean up using “Copy Rows”.

Format CSV:

1. Open both excel worksheets. Check that the data is correct, each variable has a column, and the columns for both tables are in the same order.
2. Delete the GIS generated columns “FID” and “ID”. Insert a blank column before your first column. Label it “id” and fill it with all “stable” if you’re in the stable worksheet or “unstable” in the unstable worksheet. This column is to identify whether the data represents a landslide or non-landslide point.

A	B	C	D	E	F	G	H	I	
id	lithology	landcover	aspect	slope_deg	dtb_m	dts_m	kfac	POINT_X	PC
stable	1	52	99.16	6.72	99.97	410.06	0.33	426734.5327	4
stable	1	82	343.61	1.27	83.21	360.55	0.30	426994.5327	4
stable	1	31	37.88	4.08	53.95	131.71	0.17	427254.5327	4
stable	2	41	278.14	2.53	31.09	101.24	0.46	427514.5327	4
stable	1	71	39.48	6.28	86.86	150.16	0.32	426734.5327	4

Figure 20: Screen capture showing properly formatted data columns in excel.

3. Copy and paste the unstable data directly below the stable data in excel, making sure the data are pasted into the correct attributes (shift+end+arrow key function useful here).
4. Save the csv as a new csv titled by study area “JayCooke_data.csv”.
5. Clean up numbers in excel based on personal preference, adjusting for less significant figures. It visually complicates things in R when there are more than two decimal places. Select all number data (shift+end+arrow) and decrease decimal.

6. Pay attention to column headers since the R code shared with this document through the UMN Digital Conservancy will reference these specific column names.
7. Save the files in a new folder to be used as the “active directory” when working in R and closeout of excel.

Phase 2 - Multivariate Logistic Regression Analysis in R

Download .rmd file from UMN Digital Conservancy to the folder containing the excel csv files. Set the folder as the “active directory” in R. Follow instructions to run the R-code for data prep and analysis. Most of the data, at this stage, will be in a continuous

numerical format from the raster extractions. All of the geoenvironmental factors must be converted into a categorical format. This may require looking back at the original Arc layers to recall what categories are represented by which numbers (i.e. the value of 41 on the NLCD landcover raster is equal to “Deciduous forest”).

Tips while working in R:

- It is important to save the R model output markdown to a pdf or html because, since the code includes a random sampling function, results will differ slightly for each run and overwrite any previous iterations.
- The only “knobs” to turn within the model code script outside of data prep:
    - Line 130: variables included in the Multivariate Logistic Regression (MVLR) - these can be changed after an initial run-through to show the frequency of variables chosen histogram in the analysis results after running the looped model (line 244).
    - Line 184: number of model iterations - 1000 iterations takes approximately 1 hour with ~30,000 data points (~2.2gb of information). 100 iterations takes about 3min to run with ~30,000 data input points (~ 200mb of information).
- Line 219 shows which model in the model list has the lowest AIC. To view this model’s output, click on the model list in global environments and navigate to

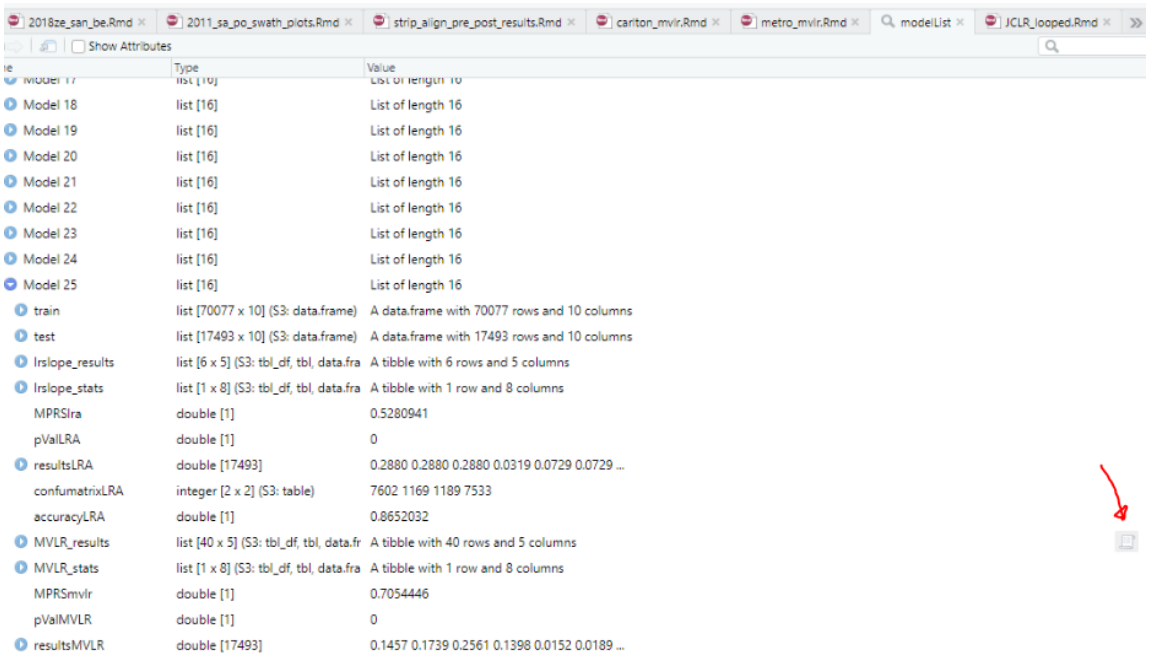

Figure 21: Model list in R, with a red arrow pointing out the scroll to access MVLR results.

the model # shown in line 219, hit the drop-down arrow for this model, and view the entire “tibble” (the scroll icon that appears to the right of the ‘MVLR_results’) OR type into the console: View(modelList[["Model ##"]][["MVLR_results"]]).

Phase 3 - Using model output to generate a susceptibility map in ArcGIS

Clean up table in excel:

Copy and paste the selected MVLR model summary results table into an excel spreadsheet (highlight the R tibble, ctrl+a copy, and paste) and save as a results table.

Filter

term	estimate	std.error	statistic	p.value
landcoverForest	1.08399202	0.6171249	1.75651963	7.899972
landcoverOpen Water	5.36800704	1.0556828	5.08486758	3.678826
landcoverShrub	1.12324579	0.7326605	1.53310552	1.252499
landcoverWetlands	1.36154019	0.7034141	1.93561677	5.291465
DTB(30,61]	0.50286104	0.3629083	1.38564210	1.658562
DTB(61,96]	0.83024778	0.3611406	2.29896019	2.150720
DTB(96,136]	0.84240152	0.3548756	2.37379386	1.760638
DTB(136,187]	1.63053808	0.3538594	4.60786993	4.068150
DTB(187,413]	1.53523461	0.3633965	4.22468220	2.392782
DTS(52,82]	0.27436931	0.2855166	0.96095762	3.365735
DTS(82,129]	0.20361442	0.2821614	0.72162397	4.705257
DTS(129,201]	-0.01001808	0.2709650	-0.03697186	9.705074
DTS(201,312]	-0.68311421	0.2926020	-2.33461889	1.956334
DTS(312,1.37e+03]	-0.66578905	0.2896596	-2.29852262	2.153206
S(4,12]	2.39367266	1.2526988	1.91081255	5.602867
S(12,23]	5.34363369	1.2083245	4.42234986	9.763319
S(23,27]	6.85957439	1.2115254	5.66193216	1.496780
S(27,32]	8.04776685	1.2259131	6.56471213	5.213348
S(32,45]	8.86834477	1.2434425	7.13209099	9.885548
KF(0.034,0.081]	1.94829671	1.1952835	1.62998717	1.031042
KF(0.081,0.146]	1.59544129	1.0910870	1.46224936	1.436729
KF(0.146,0.235]	1.37508504	0.8540269	1.61011917	1.073718
KF(0.235,0.359]	2.27491387	0.7893875	2.88187232	3.953199
KF(0.359,0.53]	1.90025682	0.8432718	2.25343332	2.423184

	Estimate	*Std. Error*	*Z-value*	*P-value*
(Intercept)	-8.66	1.46	-5.95	0.00
lithologyClay	-2.07	0.95	-2.17	0.03
lithologyDiamicton	-0.08	0.94	-0.09	0.93
lithologySand	-2.06	1.02	-2.03	0.04
landcoverDeveloped	0.78	0.75	1.04	0.30
landcoverForest	1.08	0.62	1.76	0.08
landcoverOpen Water	5.37	1.06	5.08	0.00
landcoverShrub	1.12	0.73	1.53	0.13
landcoverWetlands	1.36	0.70	1.94	0.05
DTB(30,61]	0.50	0.36	1.39	0.17
DTB(61,96]	0.83	0.36	2.30	0.02
DTB(96,136]	0.84	0.35	2.37	0.02
DTB(136,187]	1.63	0.35	4.61	0.00
DTB(187,413]	1.54	0.36	4.22	0.00
DTS(52,82]	0.27	0.29	0.96	0.34
DTS(82,129]	0.20	0.28	0.72	0.47
DTS(129,201]	-0.01	0.27	-0.04	0.97
DTS(201,312]	-0.68	0.29	-2.33	0.02
DTS(312,1.37e+03]	-0.67	0.29	-2.30	0.02
S(4,12]	2.39	1.25	1.91	0.06
S(12,23]	5.34	1.21	4.42	0.00
S(23,27]	6.86	1.21	5.66	0.00
S(27,32]	8.05	1.23	6.56	0.00
S(32,45]	8.87	1.24	7.13	0.00
KF(0.034,0.081]	1.95	1.20	1.63	0.10
KF(0.081,0.146]	1.60	1.09	1.46	0.14
KF(0.146,0.235]	1.38	0.85	1.61	0.11
KF(0.235,0.359]	2.27	0.79	2.88	0.00
KF(0.359,0.53]	1.90	0.84	2.25	0.02

Figure 22: Screen captures of the model results tibble in R (left) and the reformated table in excel (right).

Create weighted rasters using the coefficient estimates from the selected model:

1. Methods vary slightly for categorical vs continuous variables.
    a. Categorical variables:

i. Use the reclassify tool to assign each factor class their new pixel value. Since the reclassify tool will only output integers, a small work-around is to multiply all values by 100 and divide later during the raster calculation. (for example - In the case of lithology looking at the table above: All pixels in the lithology raster associated with clay should equal -207)

ii. During this stage you may notice that one category is seemingly missing from each variable. That is ok because that class or category has to be omitted to allow the regression to function (for more information, research "the dummy variable trap"). Therefore the omitted class will be given a coefficient of 0. You might also encounter classes in your raster that were not present in the analysis. These can also receive a 0 for their pixel value.

iii. As with most steps, helpful to use the Environments Tab to specify run on the Study area extent.

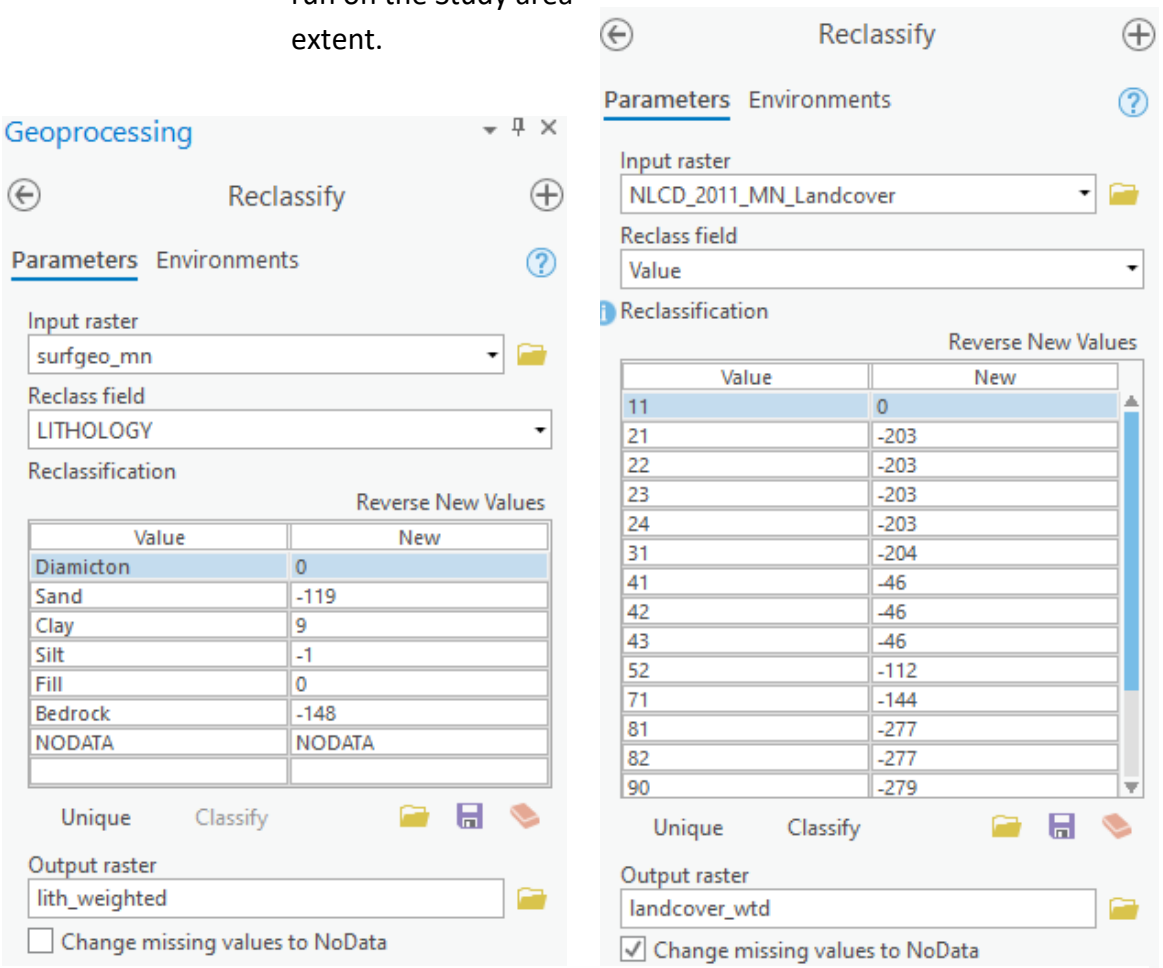

Figure 23: Screen captures showing how to created weighted rasters using the reclassify tool for lithology (left) and landcover (right).

b. Continuous variables:
    i. Adjust the symbology of the raster to match your model. In this case I use classify, geometric, with 6 bins.
    ii. Manually adjust the “start” and “end” values to match your LR model summary bins, keeping in mind that the maximum raster value could exceed your highest bin value.
    iii. Assign each group their associated coefficient with 0 for the omitted dummy variable.

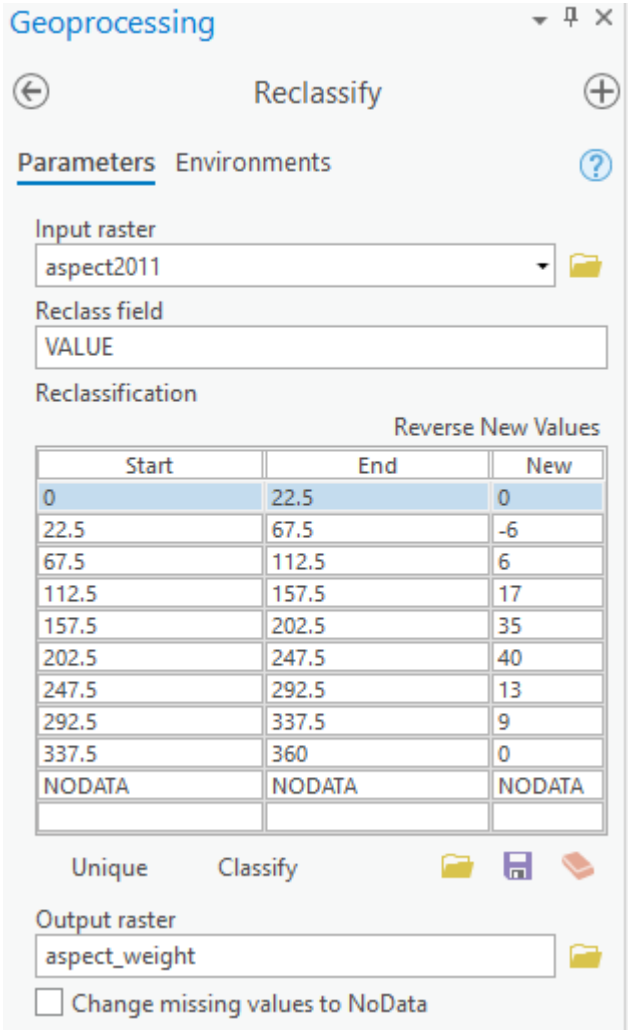

Figure 24: Screen capture showing how to reclassify a continuous variable into a weighted raster using aspect as an example.

Create a landslide susceptibility map using a raster calculation:

1. Run a raster calculation that will adjust the order of magnitude for all of the weighted rasters, sum them and incorporate our **intercept value**. This will generate the “Z raster”.
    a. Z_raster = -8.66 + ("substrate_weighted" / 100) + ("landcover_weighted" /100) + ("dtb_weighted" /100) + ("dts_weighted" /100) +("slope_weighted" /100) + ("kfactor_weighted" /100)
    b. May also need to adjust the **Environment** for raster calculator to make sure you are getting an image that isn’t too coarse - Change Cell Size from Maximum of Inputs to Minimum of Inputs.
2. To convert this into a probability raster (“P raster”) from zero to one for landslide susceptibility, perform the following raster calculation:
    a. P_raster = (Exp("Z_raster")) / (1 + Exp("Z_raster"))
3. The final raster should have pixel values that range from very close to zero up to values very close to 1. Adjust the symbology to best represent landslide susceptibility. In this project, I used the natural breaks (jenks) classification method in ArcGIS to create 3 susceptibility classes (low, moderate, and high).